BRANT AND HELMS'

FUNDAMENTALS OF DIAGNOSTIC RADIOLOGY

FIFTH EDITION

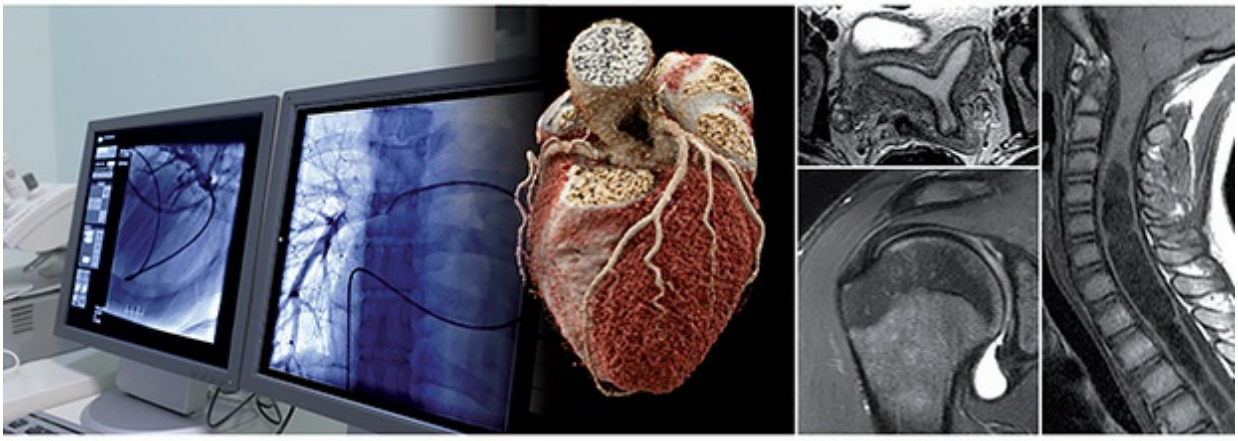

Jeffrey S. Klein
William E. Brant
Clyde A. Helms
Emily N. Vinson

Wolters Kluwer

SECTION EDITORS

SECTION I

BASIC PRINCIPLES

William E. Brant, MD, FACR
Professor Emeritus
Department of Radiology and Medical Imaging
University of Virginia School of Medicine
Charlottesville, Virginia

SECTION II

NEURORADIOLOGY

Erik H. L. Gaensler, MD
Clinical Professor
Department of Radiology and Biomedical Imaging
University of California, San Francisco
Neuroradiologist
Bay Imaging Consultants
Jerome A. Barakos, MD
Director of Neuroimaging
Department of Radiology
California Pacific Medical Center
San Francisco, California

SECTION III

CHEST

Jeffrey S. Klein, MD, FACR
A. Bradley Soule and John P. Tampas Green and Gold
Professor of Radiology
Department of Radiology
Larner College of Medicine at the University of Vermont
Burlington, Vermont

SECTION IV

BREAST RADIOLOGY

Brandi T. Nicholson, MD, FSBI
Associate Professor
Department of Radiology and Medical Imaging
University of Virginia School of Medicine
Charlottesville, Virginia

SECTION V

CARDIAC RADIOLOGY

Seth Kligerman, MD
Associate Professor
Division Chief of Cardiothoracic Radiology
Department of Radiology
University of California, San Diego
San Diego, California

SECTION VI

VASCULAR AND INTERVENTIONAL RADIOLOGY

Juan C. Camacho, MD
Assistant Attending Radiologist Interventional Radiology
Memorial Sloan Kettering Cancer Center
Assistant Professor
Department of Radiology
Weill Cornell Medical College
New York, New York
Akhilesh K. Sista, MD, FSIR
Associate Professor and Section Chief
Vascular Interventional Radiology
Department of Radiology
New York University School of Medicine
New York, New York

SECTION VII

GASTROINTESTINAL TRACT

William E. Brant, MD, FACR
Professor Emeritus
Department of Radiology and Medical Imaging
University of Virginia School of Medicine
Charlottesville, Virginia

SECTION VIII

GENITOURINARY TRACT

William E. Brant, MD, FACR
Professor Emeritus
Department of Radiology and Medical Imaging
University of Virginia School of Medicine
Charlottesville, Virginia

SECTION IX

ULTRASONOGRAPHY

William E. Brant, MD, FACR
Professor Emeritus
Department of Radiology and Medical Imaging
University of Virginia School of Medicine
Charlottesville, Virginia

SECTION X

MUSCULOSKELETAL RADIOLOGY

Clyde A. Helms, MD
Consultant
Department of Radiology
Duke University Medical Center
Durham, North Carolina
Consultant
Department of Radiology
University of New Mexico
Albuquerque, New Mexico
Emily N. Vinson, MD
Assistant Professor of Radiology
Chief, Division of Musculoskeletal Imaging
Duke University School of Medicine
Durham, North Carolina

SECTION XI

PEDIATRIC RADIOLOGY

Alan S. Brody, MD
Professor of Radiology and Pediatrics
Department of Radiology
Cincinnati Children's Hospital Medical Center
Cincinnati, Ohio
Andrew T. Trout, MD
Radiologist
Department of Radiology
Cincinnati Children's Hospital Medical Center
Cincinnati, Ohio

SECTION XII

NUCLEAR RADIOLOGY

Brett J. Mollard, MD
Body Section Co-Chief
Abdominal Imaging and Nuclear Medicine
TRA Medical Imaging
Tacoma, Washington

BRANT AND HELMS'
FUNDAMENTALS OF
DIAGNOSTIC RADIOLOGY
FIFTH EDITION

EDITORS

JEFFREY S. KLEIN, MD, FACR
A. Bradley Soule and John P. Tampas Green and Gold
Professor of Radiology
Department of Radiology
Larner College of Medicine at the University of Vermont
Burlington, Vermont

WILLIAM E. BRANT, MD, FACR
Professor Emeritus
Department of Radiology and Medical Imaging
University of Virginia School of Medicine
Charlottesville, Virginia

CLYDE A. HELMS, MD
Consultant
Department of Radiology
Duke University Medical Center
Durham, North Carolina
Consultant
Department of Radiology
University of New Mexico
Albuquerque, New Mexico

EMILY N. VINSON, MD
Assistant Professor of Radiology
Chief, Division of Musculoskeletal Imaging

Duke University School of Medicine
Durham, North Carolina

Wolters Kluwer

Philadelphia • Baltimore • New York • London
Buenos Aires • Hong Kong • Sydney • Tokyo

Acquisitions Editor: Sharon Zinner
Editorial Assistant: Dave Murphy
Marketing Manager: Julie Sikora
Production Project Manager: Joan Sinclar
Design Coordinator: Stephen Druding
Manufacturing Coordinator: Beth Welsh
Prepress Vendor: Aptara, Inc.
5th edition
Copyright © 2019 Wolters Kluwer.
1st edition © 1994 by WILLIAMS & WILKINS, 2nd edition © 1999 by WILLIAMS & WILKINS, 3rd edition © 2007 by LIPPINCOTT WILLIAMS & WILKINS, 4th edition © 2012 by LIPPINCOTT WILLIAMS & WILKINS, a WOLTERS KLUWER business

All rights reserved. This book is protected by copyright. No part of this book may be reproduced or transmitted in any form or by any means, including as photocopies or scanned-in or other electronic copies, or utilized by any information storage and retrieval system without written permission from the copyright owner, except for brief quotations embodied in critical articles and reviews. Materials appearing in this book prepared by individuals as part of their official duties as U.S. government employees are not covered by the above-mentioned copyright. To request permission, please contact Wolters Kluwer at Two Commerce Square, 2001 Market Street, Philadelphia, PA 19103, via email at permissions@lww.com, or via our website at shop.lww.com (products and services).

The following figures are copyright © Dr. Seth Kligerman (Chapter 24 figures 7, 8, 12–15, 17 and 27; Chapter 25 all figures; Chapter 26 figures 4–7, 9, 10, 16; Chapter 27 figures 7–9, 12, 13, 15, 17–18, 21–24, 27, 29 and 30; Chapter 28 all figures; Chapter 29 all figures; Chapter 30 figures 3, 4, 5, 11–20, 23, 26, 27, 29, 30–37, 39–48, 52, 55–58).

9 8 7 6 5 4 3 2 1

Printed in China

978-1-4963-6738-9
1-4963-6738-3
Library of Congress Cataloging-in-Publication Data
available upon request

This work is provided "as is," and the publisher disclaims any and all warranties, express or implied, including any warranties as to accuracy, comprehensiveness, or currency of the content of this work.

This work is no substitute for individual patient assessment based upon healthcare professionals' examination of each patient and consideration of, among other things, age, weight, gender, current or prior medical conditions, medication history, laboratory data and other factors unique to the patient. The publisher does not provide medical advice or guidance and this work is merely a reference tool. Healthcare professionals, and not the publisher, are solely responsible for the use of this work including all medical judgments and for any resulting diagnosis and treatments.

Given continuous, rapid advances in medical science and health information, independent professional verification of medical diagnoses, indications, appropriate pharmaceutical selections and dosages, and treatment options should be made and healthcare professionals should consult a variety of sources. When prescribing medication, healthcare professionals are advised to consult the product information sheet (the manufacturer's package insert) accompanying each drug to verify, among other things, conditions of use, warnings and side effects and identify any changes in dosage schedule or contraindications, particularly if

the medication to be administered is new, infrequently used or has a narrow therapeutic range. To the maximum extent permitted under applicable law, no responsibility is assumed by the publisher for any injury and/or damage to persons or property, as a matter of products liability, negligence law or otherwise, or from any reference to or use by any person of this work.

shop.lww.com

To my wife, Dr. Judy Tam, for her love, support, and encouragement, and our children, Joshua, Benjamin and Jessica, for reminding me what is most important in life.

—JEFFREY S. KLEIN, MD, FACR

I dedicate this 5th edition of our textbook to my wife, Barbara, whose love, immense patience and support makes my work on it possible, to our 10 grandchildren: Sophia, Grayson, and Noah; Danielle; Finn and Josie; Evan and Katie; Dylan and Amelia, and to the memory of my daughter, Rachel.

—WEB

To Jennifer Pohl who is the finest person I have ever known and has made me a better person in every way.

—CLYDE A. HELMS, MD

To my husband, Stephen, and our children, Allison and Matthew, who have given me all the best things in life. I wish the same for them, always.

—ENV

CONTRIBUTORS

Eric T. Aaltonen, MD, MPH
Assistant Professor
Vascular Interventional Radiology
Department of Radiology
New York University School of Medicine
New York, New York

Sarah H. Allgeier, MD, PhD
Fellow
Vascular Interventional Radiology
Department of Radiology
Medical University of South Carolina
Charleston, South Carolina

Jason J. Bailey, MD
Nuclear Medicine and Abdominal Radiologist
CMI Radiology Group
Fresno, California

Jerome A. Barakos, MD
Director of Neuroimaging
California Pacific Medical Center Sutter Health
Sutter Pacific Epilepsy Program

Spencer Behr, MD
Associate Professor of Clinical Radiology
Department of Radiology and Biomedical Imaging
University of California, San Francisco
San Francisco, California

Stephen Bracewell, MD
Resident Physician
Department of Radiology
Medical University of South Carolina
Charleston, South Carolina

William E. Brant, MD, FACR
Professor Emeritus
Department of Radiology and Medical Imaging
University of Virginia School of Medicine
Charlottesville, Virginia

Alan S. Brody, MD
Professor of Radiology and Pediatrics
Department of Radiology
Cincinnati Children's Hospital
University of Cincinnati College of Medicine
Cincinnati, Ohio

Richard K. J. Brown, MD, FACR
Professor, Department of Radiology
Director of Clinical Nuclear Medicine and Molecular Imaging
University of Michigan Health System
Ann Arbor, Michigan

Juan C. Camacho, MD
Assistant Attending Radiologist
Interventional Radiology
Memorial Sloan Kettering Cancer Center
Assistant Professor
Department of Radiology
Weill Cornell Medical College
New York, New York

Nancy A. Chauvin, MD
Associate Professor
Department of Radiology
Penn State College of Medicine
Hershey, PA

Nathaniel A. Chuang, MD
Associate Clinical Professor
Department of Radiology
University of California, San Diego
Neuroradiologist

San Diego Imaging Medical Group
San Diego, California

Marc G. Cote, DO, FACOI, FACP
Assistant Dean for Clinical Education
Associate Professor of Internal Medicine
Pacific Northwest University of Health Sciences
College of Osteopathic Medicine
Yakima, Washington

Bradley Fehrenbach, MD
Nuclear Radiologist
Diversified Radiology
Denver, Colorado

Robert R. Flavell, MD, PhD
Assistant Professor in Residence
Department of Radiology and Biomedical Imaging
Section of Nuclear Medicine
University of California, San Francisco
San Francisco, California

Robert J. Fleck, Jr., MD
Associate Professor
Department of Radiology
Cincinnati Children's Hospital Medical Center
University of Cincinnati
Cincinnati, Ohio

Carl Gunnar Forsberg, MD
Resident Physician
Department of Radiology
Medical University of South Carolina
Charleston, South Carolina

Erik H. L. Gaensler, MD
Clinical Professor
Department of Radiology and Biomedical Imaging
University of California, San Francisco

Neuroradiologist
Bay Imaging Consultants

Arpit Gandhi, MD
Radiology resident
Christiana Care Health System
Newark, Delaware

Alisa D. Gean, MD
Professor Emeritus
Department of Radiology and Biomedical Imaging
University of California, San Francisco
San Francisco, California

Curtis E. Green, MD
Professor of Radiology and Cardiology
Department of Radiology
Larner College of Medicine at the University of Vermont
Burlington, Vermont

Marcelo Guimaraes, MD, FSIR
Professor and Director
Vascular Interventional Radiology
Department of Radiology
Medical University of South Carolina
Charleston, South Carolina

Aishwarya Gulati, MD
Resident Physician
Department of Internal Medicine
Carle Foundation Hospital
Urbana, Illinois

Kate Hanneman, MD, MPH, FRCPC
Assistant Professor
Department of Medical Imaging, Toronto General Hospital
University of Toronto
Toronto, Canada

Peter A. Harri, MD
Assistant Professor
Abdominal Imaging
Department of Radiology and Imaging Sciences
Emory University School of Medicine
Atlanta, Georgia

Heather Hartung, RN-BSN
RN Patient Navigator
Vascular Interventional Radiology
Medical University of South Carolina
Charleston, South Carolina

Clyde A. Helms, MD
Consultant
Department of Radiology
Duke University Medical Center
Durham, North Carolina
Consultant
Department of Radiology
University of New Mexico
Albuquerque, New Mexico

Cash Jeremy Horn, MD
Assistant Professor
Vascular Interventional Radiology
Department of Radiology
New York University School of Medicine
New York, New York

Michael J. Horowitz, MD, PhD
Cardiothoracic Imaging Fellow
Department of Radiology
UC San Diego Medical Center
San Diego, California

Albert Hsiao, MD, PhD
Assistant Professor
Department of Radiology

UC San Diego
La Jolla, California

Kathleen Jacobs, MD
Assistant Professor
Department of Radiology
University of California, San Diego
San Diego, California

Blaise V. Jones, MD
Chief, Neuroradiology
Cincinnati Children's Hospital Medical Center
Professor
University of Cincinnati School of Medicine
Cincinnati, Ohio

Vivek Kalia, MD, MPH, MS
Assistant Professor of Radiology
Department of Radiology
Division of Musculoskeletal Radiology
University of Michigan Health System
Ann Arbor, Michigan

Asef Khwaja, MD
Assistant Professor of Radiology
Department of Radiology
The Children's Hospital of Philadelphia. Perelman School of Medicine at the University of Pennsylvania
Philadelphia, Pennsylvania

Jeffrey S. Klein, MD, FACR
A. Bradley Soule and John P. Tampas Green and Gold
Professor of Radiology
Department of Radiology
Larner College of Medicine at the University of Vermont
Burlington, Vermont

Seth Kligerman, MD
Associate Professor

Division Chief of Cardiothoracic Radiology
Department of Radiology
University of California, San Diego
San Diego, California

Nima Kokabi, MD
Assistant Professor
Interventional Radiology and Image-guided Medicine
Department of Radiology and Imaging Sciences
Emory University School of Medicine
Atlanta, Georgia

Kelly K. Koeller, MD, FACR
Associate Professor
Department of Radiology
Mayo Clinic
Rochester, MN and
Chief, Neuroradiology
American Institute for Radiologic Pathology
Silver Spring, Maryland

Tuong H. Le, MD, PhD
Brain and Spine Imaging Consultants (BASIC)
Dallas, Texas

Jay S. Leb, MD
Assistant Professor
Department of Radiology
Columbia University Medical Center
New York, New York

Clayton Li, MD
Resident Physician
Department of Radiology
New York University School of Medicine
New York, New York

Jeffrey P. Lin, MD, PhD
Nuclear Radiologist

TRA Medical Imaging
Tacoma, Washington

Camilla E. Lindan, MD
Assistant Clinical Professor
Department of Radiology
University of California San Francisco
Department of Diagnostic Imaging
Kaiser Hospital, San Francisco, California

Louis G. Martin, MD, FACR, FSIR
Emeritus Professor
Interventional Radiology and Image-guided Medicine
Department of Radiology and Imaging Sciences
Emory University School of Medicine
Atlanta, Georgia

Meredith McDermott, MD
Assistant Professor
Vascular Interventional Radiology
Department of Radiology
New York University School of Medicine
New York, New York

Pardeep K. Mittal, MD, FACR
Professor
Body Imaging
Department of Radiology and Imaging
Medical College of Georgia
Augusta, Georgia

Brett J. Mollard, MD
Body Section Co-Chief
Abdominal Imaging and Nuclear Medicine
TRA Medical Imaging
Tacoma, Washington

Govind Mukundan, MD
Neuroradiology Section

Sutter Imaging
Sacramento, California

Christopher A. Mutch, MD, PhD
Radiologist
Bay Imaging Consultants
Walnut Creek, California

Usha D. Nagaraj, MD
Assistant Professor of Clinical Radiology and Pediatrics
Cincinnati Children's Hospital Medical Center/ University of Cincinnati College of Medicine
Cincinnati, Ohio

Jonathan V. Nguyen, MD
Assistant Professor
Department of Radiology
University of Virginia Health System
Charlottesville, Virgina

Brandi T. Nicholson, MD, FSBI
Associate Professor
Department of Radiology and Medical Imaging
University of Virginia School of Medicine
Charlottesville, Virginia

Walter L. Olsen, MD, FACR
San Diego Imaging Medical Group
San Diego, California

Amish Patel, MD
Assistant Professor
Vascular Interventional Radiology
Department of Radiology
New York University School of Medicine
New York, New York

Jonathan David Perry, MD
Chief Resident

Department of Radiology
Medical University of South Carolina
Charleston, South Carolina

Jennifer Pohl, PhD, MD
Associate Professor
Department of Radiology
University of New Mexico
Albuquerque, New Mexico

Derk D. Purcell, MD
Assistant Clinical Professor
Department of Radiology and Biomedical Imaging
University of California, San Francisco
California Pacific Medical Center
San Francisco, California

Carrie M. Rochman, MD
Assistant Professor
Department of Radiology and Medical Imaging
University of Virginia Health System
Charlottesville, Virginia

Howard A. Rowley, MD
Joseph Sackett Professor of Radiology
Professor of Radiology, Neurology, and Neurosurgery
University of Wisconsin
Madison, Wisconsin

Claudio Schonholz
Professor
Vascular Interventional Radiology
Department of Radiology
Medical University of South Carolina
Charleston, South Carolina

David J. Seidenwurm, MD
Network Medical Director
Quality Committee Chair

Sutter Medical Foundation
Sacramento, California

Robert Y. Shih, MD
Assistant Professor
Department of Radiology
Uniformed Services University
Bethesda, Maryland

Akhilesh K. Sista, MD, FSIR
Associate Professor and Section Chief Vascular Interventional Radiology
Department of Radiology
New York University School of Medicine
New York, New York

Ethan A. Smith, MD
Associate Professor
Department of Radiology
Cincinnati Children's Hospital Medical Center
University of Cincinnati College of Medicine
Cincinnati, Ohio

Divya Sridhar, MD
Assistant Professor
Vascular Interventional Radiology
Department of Radiology
New York University School of Medicine
New York, New York

Judy K. Tam, MD
Associate Professor of Radiology
Department of Radiology
Larner College of Medicine at the University of Vermont
Burlington, Vermont

Anobel Tamrazi, MD, PhD
Interventional Radiology
Palo Alto Medical Foundation
Redwood City, California

Bedros Taslakian, MD
Assistant Professor
Vascular and Interventional Radiology
Department of Radiology
New York University School of Medicine
New York, New York

Andrew T. Trout, MD
Associate Professor of Radiology
Cincinnati Children's Hospital Medical Center
Cincinnati, Ohio

Emily N. Vinson, MD
Assistant Professor of Radiology
Chief, Division of Musculoskeletal Imaging
Duke University School of Medicine
Durham, North Carolina

Vibhor Wadhwa, MD
Radiology Resident
Department of Radiology
University of Arkansas for Medical Sciences
Little Rock, Arkansas

Alyssa T. Watanabe, MD
Clinical Associate Professor
Neuroradiology Division
USC Keck School of Medicine
Los Angels, California

Elizabeth Weihe, MD
Associate Professor
Department of Radiology
University of California-San Diego
San Diego, California

Ricardo Tadayoshi Barbosa Yamada, MD
Assistant Professor
Vascular Interventional Radiology

Department of Radiology
Medical University of South Carolina
Charleston, South Carolina

PREFACE

Much has changed in radiology since Fundamentals of Diagnostic Radiology by Brant and Helms was first conceived in the late 1980s as an aide to radiology residents studying for their radiology oral board examinations. In the past 30 years, the amount of information dispensed during radiology residency has increased dramatically, and there has been an explosion in technology including advances in multidetector and coned-beam computed tomography, magnetic resonance imaging, nuclear medicine, and ultrasound. The past 10 to 15 years have seen the development of new imaging modalities including digital tomosynthesis, dual-energy subtraction radiography, functional/metabolic imaging, and the birth of interventional oncology with new image-guided treatment techniques including thermal tumor ablation and targeted transcatheter treatment of neoplasms. In the United States an examination taken by residents in their 36th month of training has in part replaced the old oral examinations for those seeking diagnostic radiology certification by the American Board of Radiology. Despite a multitude of online sources of information for radiology residents, there remains a need for basic, high-quality introductory material that spans all diagnostic radiology subspecialties.

This fifth edition of Brant and Helms' Fundamentals of Diagnostic Radiology contains significantly expanded and revised sections dedicated to breast radiology, cardiac imaging, vascular/interventional radiology, pediatric radiology, and nuclear medicine that reflect the growing fund of knowledge in these subspecialties and their increased importance in radiology resident curricula. We are fortunate to have six new section editors who have contributed their expertise to this new edition and have invited contributions from many recently trained radiologists in creating an updated version of core material. Dr. Brandi T. Nicholson, a breast radiologist and Associate Residency Program Director for the diagnostic residency program at the University of Virginia Health System has created a section that covers screening, diagnostic, and interventional breast radiology. Dr. Seth Kligerman, Section Chief of Cardiothoracic Imaging at the University of California, San Diego, shares his knowledge and experience in cardiovascular imaging in a significantly expanded Cardiac section. The Vascular and Interventional Radiology section, edited by Drs. Akhilesh Sista of NYU Langone Medical Center and Juan Camacho of the Memorial Sloan Kettering

Cancer Center in New York provides a thorough introduction to the spectrum of image-guided vascular and nonvascular interventions including the interventional treatment of hepatic malignancies. Drs. Alan Brody and Andrew Trout of the Cincinnati Children's Hospital Medical Center have significantly revised the section on Pediatric Radiology. The Nuclear Medicine section, edited by Dr. Brett J. Mollard of Diagnostic Imaging Northwest, is completely revised with a more condensed review of common nuclear medicine topics.

Those familiar with previous editions will recognize editors and authors Drs. William Brant and Clyde Helms, who developed the concept of Fundamentals of Diagnostic Radiology 30 years ago. For this fifth edition, Bill has updated his introductory chapter on diagnostic imaging methods and contributed updated material on gastrointestinal and genitourinary radiology and ultrasound. Clyde has updated his section on Musculoskeletal Imaging along with Dr. Emily Vinson, Division Chief of Musculoskeletal Imaging at Duke University Medical Center, who now joins as an editor of Fundamentals. Drs. Erik Gaensler and Jerome Barakos have returned to edit the revised Neuroradiology section. Dr. Jeffrey Klein, along with colleagues from the Larner College of Medicine at the University of Vermont, provides an updated section on Chest Radiology and is now a senior editor of Brant and Helms' Fundamentals of Diagnostic Radiology.

The editors of Fundamentals would like to acknowledge the efforts of the staff of Wolters Kluwer who have supported this new edition and helped guide it to successful completion. Sharon Zinner, Senior Acquisitions Editor at Wolters Kluwer Health, has lent her steady hand and vast experience with radiology textbooks to this major revision. David Murphy, Senior Managing Editor at Wolters Kluwer Health, has kept everyone on task over the past 2 years. Indu Jawwad, Senior Project Manager and Joan Sinclair, Production Manager, have worked closely with the editors and authors during the proofing and final editing stages of the book.

—Jeffrey S. Klein, MD, FACR
—William E. Brant, MD, FACR
—Clyde A. Helms, MD
—Emily N. Vinson, MD

CONTENTS

SECTION III

CHEST

SECTION EDITOR: Jeffrey S. Klein

SECTION IV

BREAST RADIOLOGY

SECTION EDITOR: Brandi T. Nicholson

SECTION VI

VASCULAR AND INTERVENTIONAL RADIOLOGY

SECTION EDITORS: Juan C. Camacho and Akhilesh K. Sista

SECTION VII
GASTROINTESTINAL TRACT

SECTION EDITOR: William E. Brant

SECTION VIII
GENITOURINARY TRACT

SECTION EDITOR: William E. Brant

SECTION EDITOR: Brett J. Mollard

LIST OF UNIVERSAL ABBREVIATIONS

Abbreviations for use throughout Klein/Brant/Helms/Vinson, Fundamentals of Diagnostic Radiology, 5th Edition.

AIDS	Acquired immunodeficiency Syndrome
CNS	Central nervous system
CT	Computed tomography
CSF	Cerebrospinal fluid
CXR	Conventional chest radiograph
DWI	Diffusion weighted imaging (MR)
FDG	18-F-fluorodeoxyglucose
GRE	Gradient-echo MR imaging
GI	Gastrointestinal
HIV	Human immunodeficiency virus
HRCT	High resolution chest CT
HU	Hounsfield unit – a reference scale for CT
IV	Intravenous
LA	Left atrium
LV	Left ventricle
MDCT	Multi-detector computed tomography
MR	Magnetic resonance imaging
PA	Pulmonary artery
PET	Positron emission tomography
PET-CT	Positron emission tomography – computed tomography
SPECT	Single-photon emission computed tomography
RA	Right atrium
RV	Right ventricle
T1WI	T1-weighted image (MR)
T2WI	T2-weighted image (MR)
US	Ultrasound

SECTION I

BASIC PRINCIPLES

SECTION EDITOR: William E. Brant

CHAPTER 1 DIAGNOSTIC IMAGING METHODS

WILLIAM E. BRANT

Diagnostic radiology is a dynamic specialty that continues to undergo rapid change with ongoing advancements in utilization and technology. Not only has the number of imaging methods increased, but each one continues to undergo improvement and refinement of its use in medical diagnosis. This chapter reviews the basics of the major diagnostic imaging methods and provides the basic principles of image interpretation for each method. Contrast agents commonly used in diagnostic radiology are discussed. The basics of nuclear radiology are discussed in later chapters.

CONVENTIONAL RADIOGRAPHY

Conventional radiographic examination of the human body dates back to the genesis of diagnostic radiology in 1895 when Wilhelm Roentgen produced the

first x-ray film image of his wife's hand. Conventional radiography remains fundamental to the practice of diagnostic imaging.

Image Generation. X-rays are a form of radiant energy similar in many ways to visible light. X-rays differ from visible light in that they have a very short wavelength and are able to penetrate many substances that are opaque to light. The x-ray beam is produced by bombarding a tungsten target with an electron beam within an x-ray tube.

Film Radiography. Conventional film radiography utilizes a screen-film system within a film cassette as the x-ray detector. As x-rays pass through the human body they are attenuated by interaction with body tissues (absorption and scatter) and produce an image pattern on film that is recognizable as human anatomy. X-rays transmitted through the patient bombard a fluorescent particle–coated screen within the film cassette causing a photochemical interaction that emits light rays, which expose photographic film within the cassette (Fig. 1.1). The film is removed from the cassette and developed by an automated chemical film processor. The final product is an x-ray image of the patient's anatomy on a film (Fig. 1.2).

Computed radiography (CR) is a filmless system that eliminates chemical processing and provides digital radiographic images. CR substitutes a phosphor imaging plate for the film-screen cassette. CR cassette sizes match those available for traditional film-screen cassettes. The same gantry, x-ray tube, and exposure control systems, and cassette holders used in conventional radiography are utilized for CR. The phosphor-coated imaging plate interacts with x-rays transmitted through the patient to capture a latent image. The phosphor plate is placed within a reading device that scans the plate with a helium-neon laser, emitting light, which is captured by a photomultiplier tube and processed into a digital image. The CR receptor is erased with white light and is used repeatedly. The digital image is transferred to a computerized picture archiving and communication system (PACS). The PACS stores and transmits digital images via computer networks to give physicians and healthcare providers in many locations simultaneous instant access to the diagnostic images.

Digital radiography (DR) provides a filmless and cassetteless system for capturing x-ray images in digital format. DR substitutes a fixed electronic detector or charge-coupled device (CCD) for the film-screen cassette or phosphor imaging plate. Direct read-out detectors produce an immediate digital radiographic image. Most DR detectors are installed in a fixed gantry

limiting the ability of the system to obtain images portably at the patient's bedside. CR is generally used for that purpose in a digital imaging department. Direct digital image capture is particularly useful for angiography providing rapid digital image subtraction and for fluoroscopy and image-guided interventional procedures capturing video images with low, continuous radiation.

Fluoroscopy enables real-time radiographic visualization of moving anatomic structures. A continuous x-ray beam passes through the patient and falls onto a digital radiographic system. The digital images are displayed in real time on a television monitor, and are recorded digitally as a movie clip or as a series of images. Fluoroscopy is extremely useful to evaluate motion such as swallowing, intestinal peristalsis, movement of the diaphragm with respiration, and cardiac action. Fluoroscopy is also used to perform and monitor continuously radiographic procedures such as barium studies, catheter placements, and other interventional procedures. Video and static fluoroscopic images are routinely stored in digital format on a PACS for retrospective interpretation and documentation.

Conventional angiography involves the opacification of blood vessels by intravascular injection of iodinated contrast agents. **Conventional arteriography** uses small flexible catheters that are placed in the arterial system usually via puncture of the femoral artery in the groin. With the use of fluoroscopy for guidance, catheters of various sizes and shapes can be manipulated selectively into virtually every major artery. Contrast injection is performed by hand or by mechanical injector and is accompanied by digital computer acquisition (DR) of the fluoroscopic image. The result is a timed series of images depicting contrast flow through the artery injected and the tissues perfused. **Conventional venography** is performed by contrast injection of veins via distal puncture or selective catheterization.

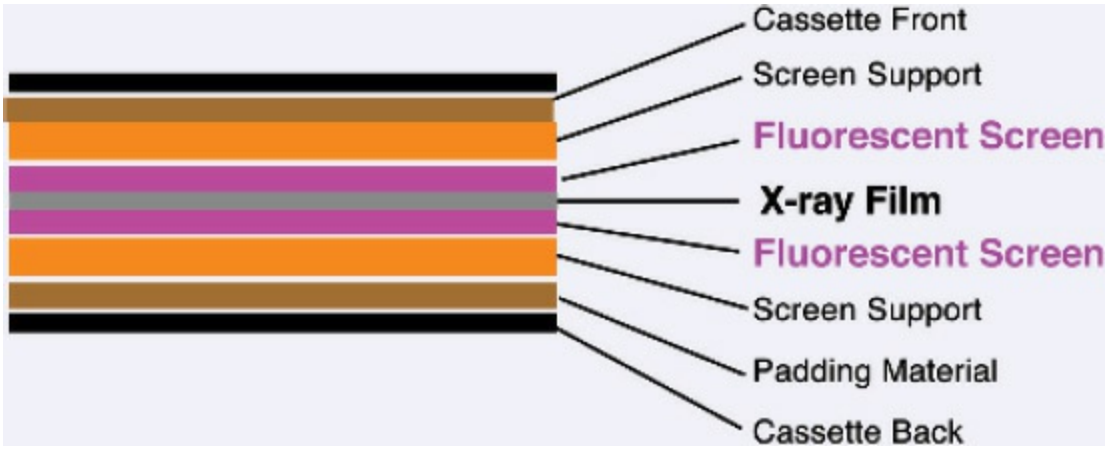

FIGURE 1.1. X-Ray Film Cassette. Diagram demonstrates a sheet of x-ray film between two fluorescent screens within a light-proof cassette.

Naming Radiographic Views. Most radiographic views are named on the basis of the direction that the x-ray beam passes through the patient. A posteroanterior (PA) chest radiograph is one in which the x-ray beam passes through the back of the patient and exits through the front of the patient to expose an x-ray detector positioned against the patient's chest. An anteroposterior (AP) chest radiograph is exposed by an x-ray beam passing through the patient from front to back. A craniocaudad (CC) mammogram is produced by passing a beam through the breast in a vertical, cranial to caudad, direction with the patient standing or sitting. Views are additionally named by identifying the position of the patient. Erect, supine, or prone views may be specified. A right lateral decubitus view of the chest is exposed with a horizontal x-ray beam passing through the chest of a patient lying on his or her right side. Radiographs taken during fluoroscopy are named on the basis of the patient's position relative to the fluoroscopic table because the x-ray tube is positioned beneath the table. A right posterior oblique (RPO) view is taken with the patient lying with the right side of his or her back against the table and the left side elevated away from the table. The x-ray beam generated by the x-ray tube located beneath the table passes through the patient to the x-ray detector located above the patient.

Principles of Interpretation. Conventional radiographs demonstrate five basic radiographic densities: air, fat, soft tissue, bone, and metal (or x-ray contrast agents). Air attenuates very little of the x-ray beam, allowing nearly the full force of the beam to pass through the patient and blacken the radiographic image. Bone, metal, and radiographic contrast agents attenuate a large proportion of the x-ray beam, allowing very little radiation through to

blacken the image. Thus, bone, metallic objects, and structures opacified by x-ray contrast agents appear white on radiographs. Fat and soft tissues attenuate intermediate amounts of the x-ray beam, resulting in proportional degrees of image blackening (shades of gray). Soft tissue attenuates more radiation than fatty tissues. Thick structures attenuate more radiation than thin structures of the same composition. Anatomic structures are seen on radiographs when they are outlined in whole or in part by tissues of different x-ray attenuation. Air in the lung outlines pulmonary vascular structures, producing a detailed pattern of the lung parenchyma (Fig. 1.3). Fat within the abdomen outlines the margins of the liver, spleen, and kidneys, allowing their visualization (Fig. 1.2B). The high density of bones enables visualization of bone details through overlying soft tissues (Figs. 1.2B and 1.3). Metallic objects such as surgical clips are usually clearly seen because they highly attenuate the x-ray beam. Radiographic contrast agents are suspensions of iodine or barium compounds that highly attenuate the x-ray beam and are used to outline anatomic structures. Disease states may obscure normally visualized anatomic structures by silhouetting their outline. Pneumonia in the right middle lobe of the lung replaces air in the alveoli with fluid and pus silhouetting the right heart border (Fig. 1.4).

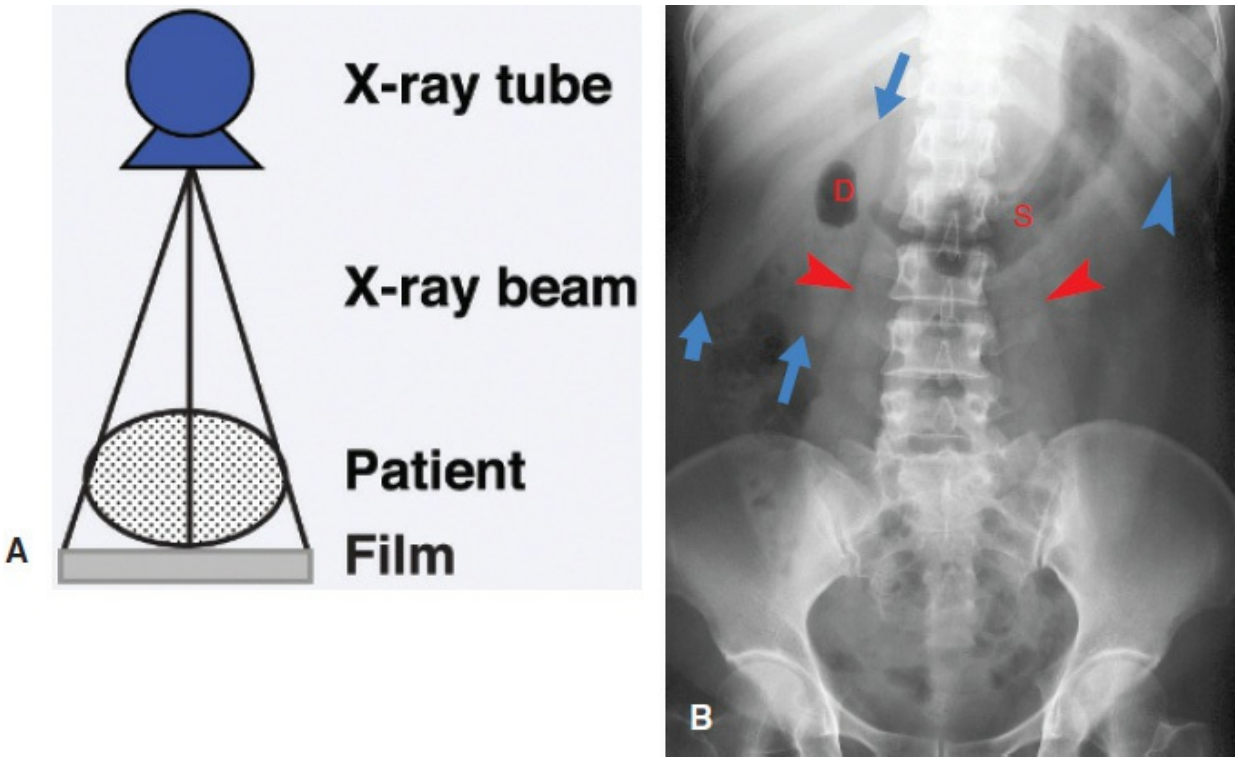

FIGURE 1.2. Conventional Radiography. A: Diagram of an x-ray tube producing x-rays that pass through the patient and expose the radiographic film. For digital radiography a phosphor imaging plate or fixed electronic detector takes the place of the film cassette. **B:** Supine AP (anteroposterior) radiograph

of the abdomen reveals the patient's anatomy because anatomic structures differ in their capacity to attenuate x-rays that pass through the patient. The stomach (S) and duodenum (D) are visualized because air in the lumen is of lesser radiographic density than the soft tissues that surround the GI tract. The right kidney (between thin blue arrows), edge of the liver (fat blue arrow), edge of the spleen (blue arrowhead), and both psoas muscles (red arrowheads) are visualized because lower attenuation fat outlines the soft tissue density of these structures. The bones of the ribs, spine, pelvis, and hips are clearly seen through the soft tissues because of their high radiographic density.

CROSS-SECTIONAL IMAGING TECHNIQUES

CT, MR, and US are techniques that produce cross-sectional images of the body. All three interrogate a three-dimensional volume or slice of patient tissue to produce a two-dimensional image. The resulting image is made up of a matrix of picture elements (pixels), each of which represents a volume element (voxel) of patient tissue. The tissue composition of the voxel is averaged (volume averaged) for display as a pixel. CT and MR assign a numerical value to each picture element in the matrix. The matrix of picture elements that make up each image is usually between 256 × 256 (65,536 pixels) to 1,024 × 1,024 (1,048,576 pixels) determined by the specified acquisition parameters (Fig. 1.5).

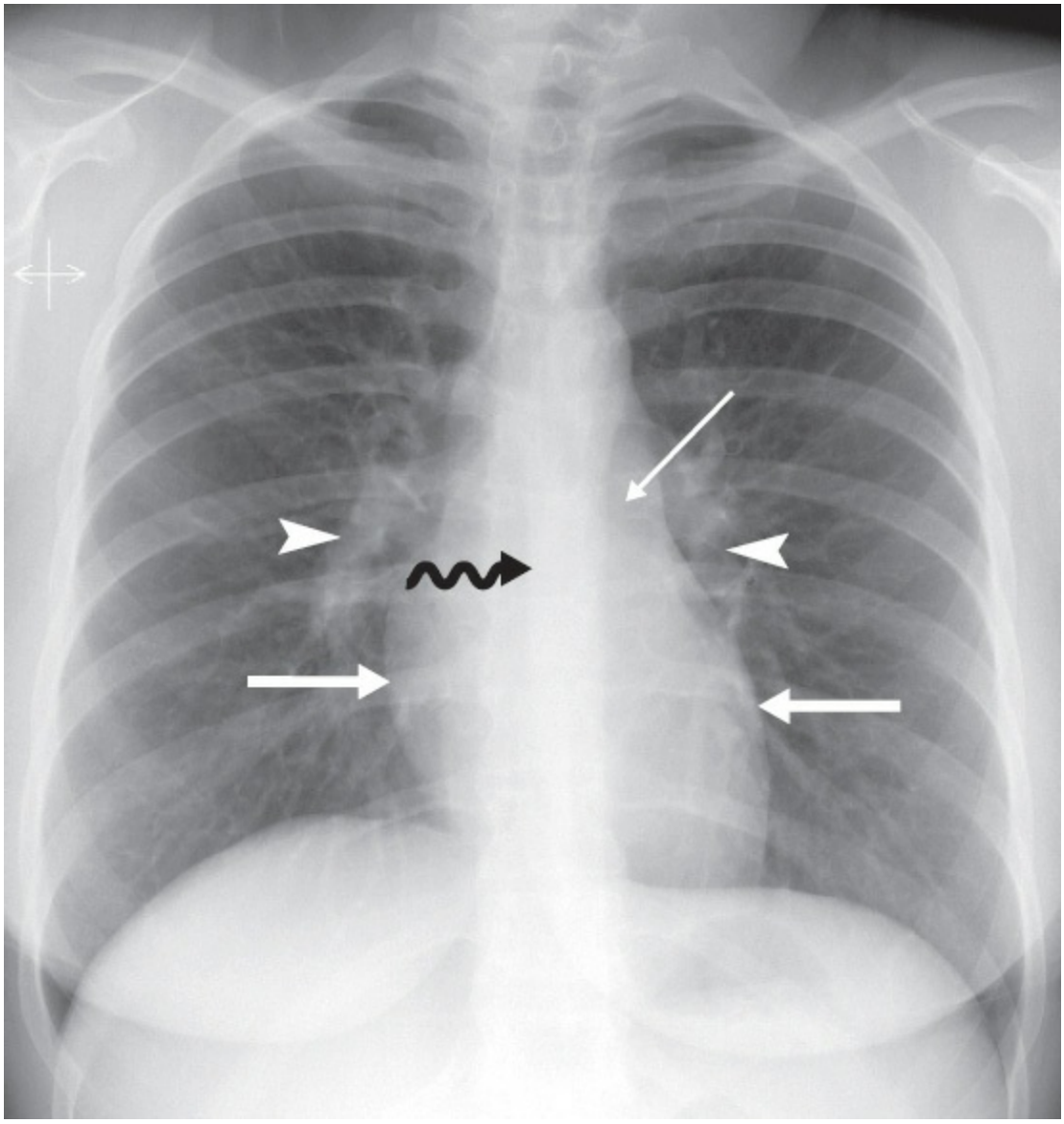

FIGURE 1.3. Erect PA Chest Radiograph. The pulmonary arteries (arrowheads) are seen in the lung because the vessels are outlined by air in alveoli. Both cardiac border (fat arrows) are crisply defined by adjacent air-filled lung. The left main bronchus (skinny arrow) is seen because its air-filled lumen is surrounded by soft tissue of the mediastinum. The azygoesophageal recess (squiggly arrow) is well defined by air-filled lung of the right lower lobe.

To produce an anatomic image, shades of gray are assigned to ranges of pixel values. For example, 16 shades of gray may be divided over a window width of 320 pixel values (Fig. 1.6). Groups of 20 pixel values are each assigned one of the 16 gray shades. The middle gray shade is assigned to the pixel values centered on a selected window level. Pixels with values greater than the upper limit of the window width are displayed white, and pixels with values less than the lower limit of the window width are displayed black. To analyze optimally all of the anatomic information of any particular slice, the

image is viewed at different window-width and window-level settings optimized for bone, air-filled lung, soft tissue, and so forth (Fig. 1.7).

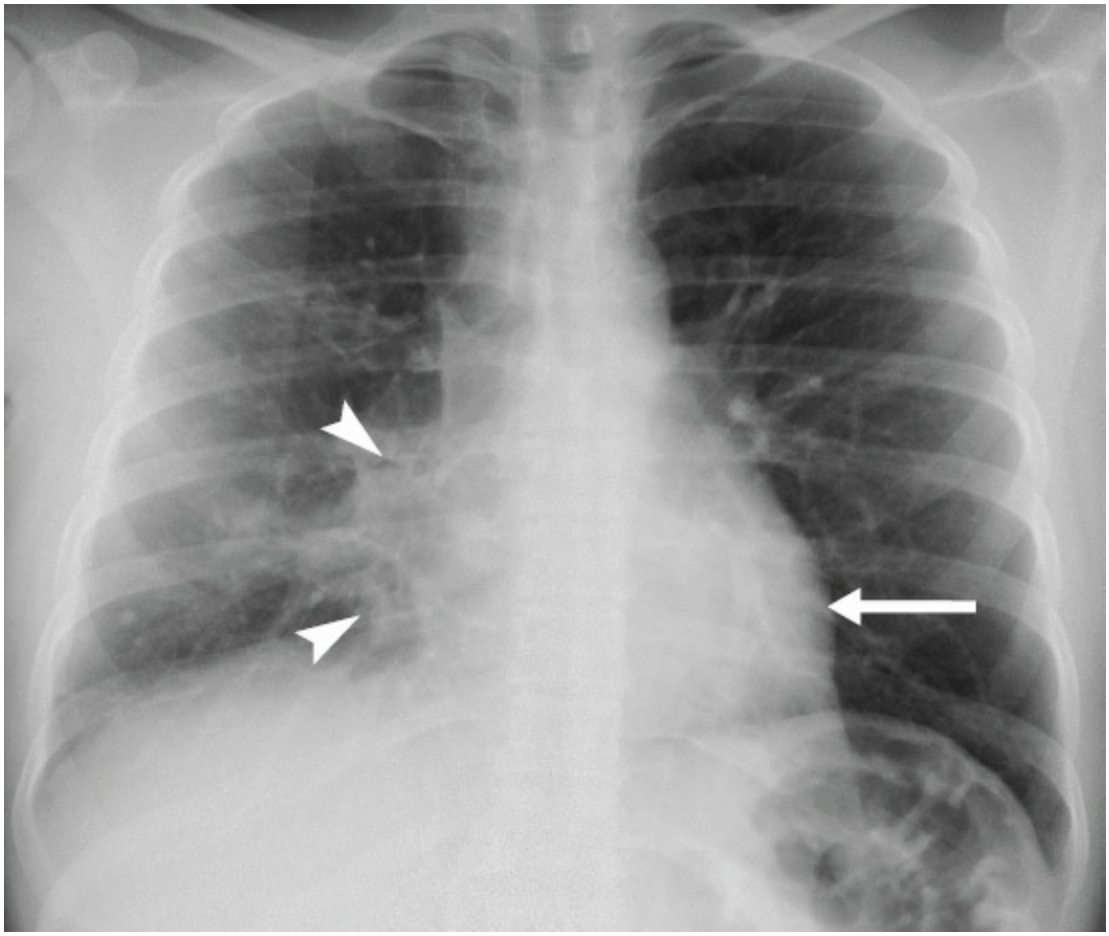

FIGURE 1.4. Right Middle Lobe Pneumonia. PA erect chest radiograph demonstrates pneumonia (arrowheads) in the right middle lobe replacing the lucency of air in the lung with soft tissue density and silhouetting the right heart border. Note the normal sharp definition of the left heart border (arrow) defined by the normal air-containing lingula.

The digital images obtained by CT, MR, and US examination are ideal for storage and access on PACS. Current PACS allow a broad range of image manipulation while viewing and interpreting images. Among the features that can be used are scrolling, interactive alterations in window width and window level, magnification, fusing of images from different modalities, reformatting serial images in different anatomic planes, creating three-dimensional reconstructions, and marking key images that summarize major findings.

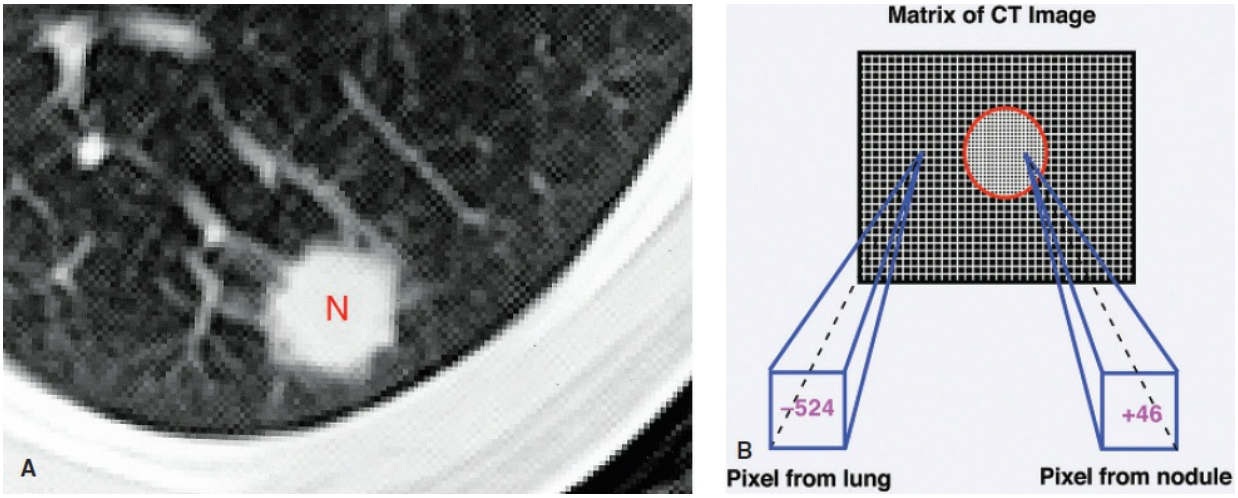

FIGURE 1.5. Image Matrix. A: Magnified CT image of a pulmonary nodule (N). The pixels that make up the image are evident as tiny squares within the image. The window width is set at 2,000 H with a window level of –600 H to accentuate visualization of the white soft tissue nodule on a background of gray, air-filled lung. **B:** Diagram of the matrix that constitutes the CT image. A pixel from air-filled lung with a calculated CT number of –524 H is gray, whereas a pixel from the soft tissue nodule with a calculated CT number of +46 H is white.

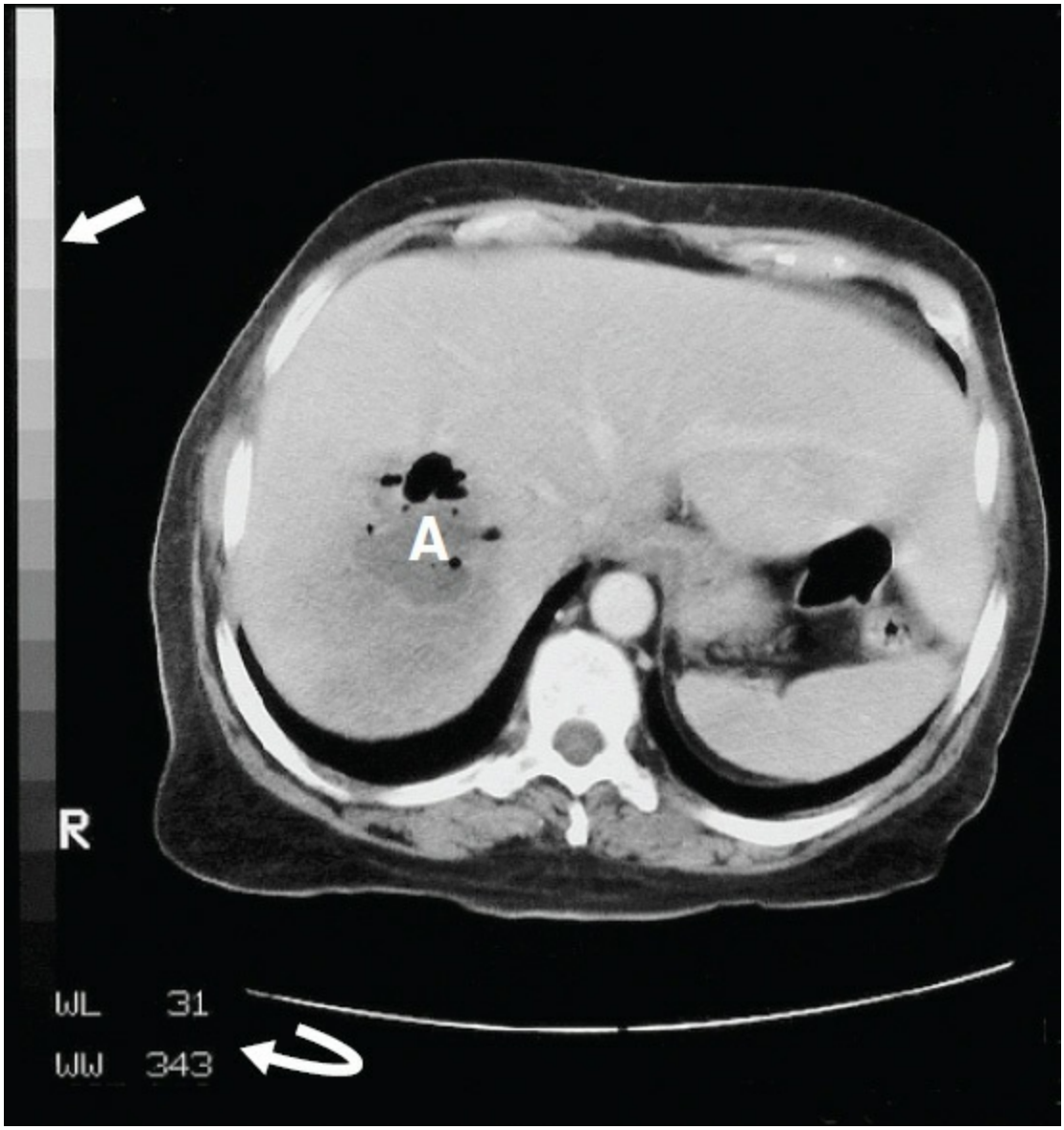

FIGURE 1.6. Gray Scale. A CT image of the abdomen includes a gray scale (straight arrow) along its left edge. Each individual pixel in the CT image is assigned a shade of gray depending on its calculated CT number (H unit) and the window width and window level (WW, WL, curved arrow) selected by the CT operator. Pure white and pure black are at the top and bottom of the gray scale. R indicates the patient's right side. Cross-sectional images in the transverse plane are routinely viewed from "below," as if standing at the patient's feet. This orientation allows easy correlation with conventional radiographs, which are routinely viewed as if facing the patient with the patient's right side to the viewer's left. This patient has an abscess (A) in the liver.

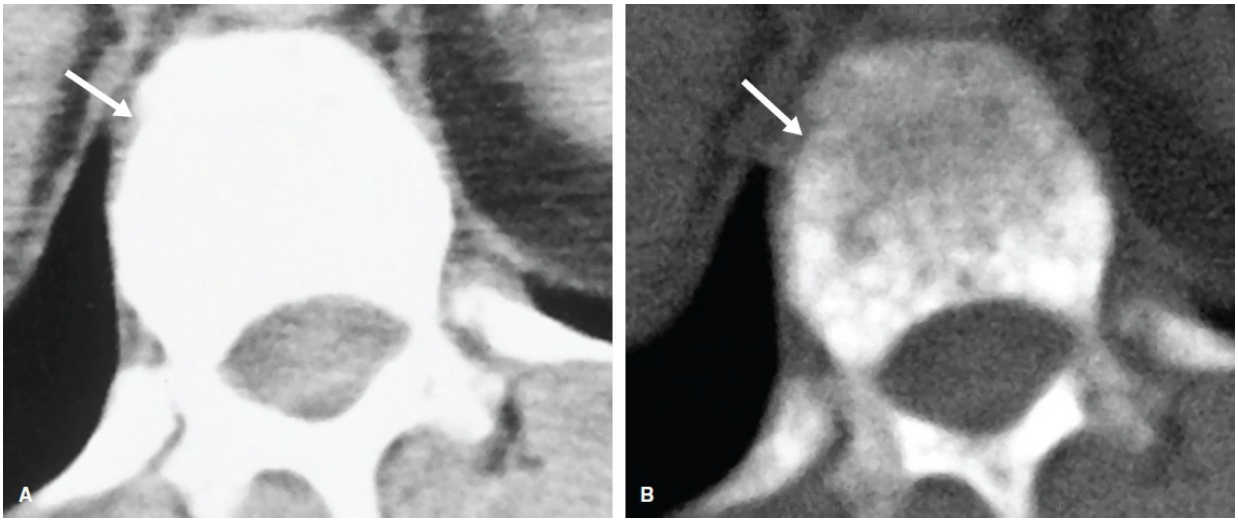

FIGURE 1.7. CT Windows. A: A CT image of a lower thoracic vertebral body photographed with "soft tissue windows" (window width = 482 H, window level = –14 H) portrays a thoracic vertebra (arrow) entirely white with no bone detail. **B:** The same CT image rephotographed with "bone windows" (window width = 2,000 H, window level = 400 H) demonstrates destructive changes in the vertebral body (arrow) owing to metastatic lung carcinoma.

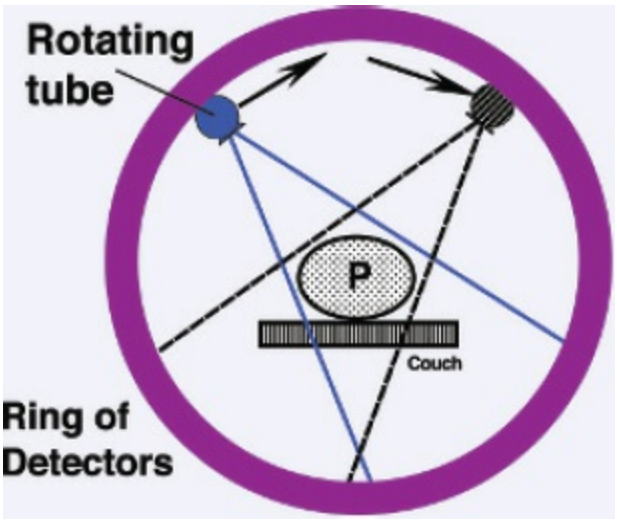

FIGURE 1.8. Computed Tomography. Diagram of a CT scanner. The patient (P) is placed on an examination couch within the core of the CT unit. An x-ray tube rotates around the patient, producing pulses of radiation that pass through the patient. Transmitted x-rays are detected by a bank of radiation detectors opposite the x-ray tube. X-ray transmission data are sent to a computer, which uses an assigned algorithm to calculate the matrix of CT numbers used to produce the anatomic cross-sectional image. With helical CT scan technique, the patient couch moves the patient continuously through the rotating x-ray beam. With multidetector CT, multiple image slices are obtained simultaneously as the patient is moved through the scanner.

Computed Tomography

CT uses a computer to reconstruct mathematically a cross-sectional image of the body from measurements of x-ray transmission through thin slices of patient tissue. A narrow, well-collimated beam of x-rays is generated on one side of the patient (Fig. 1.8). The x-ray beam is attenuated by absorption and scatter as it passes through the patient. Sensitive detectors on the opposite side of the patient measure x-ray transmission through the slice. These measurements are systematically repeated many times from different directions while the x-ray tube is pulsed as it rotates around the patient. CT numbers are assigned to each pixel in the image by a computer algorithm that uses as data these measurements of transmitted x-rays. CT pixel numbers are proportional to the difference in average x-ray attenuation of the tissue within the voxel compared with that of water. A Hounsfield unit (H) scale, named for Sir Godfrey Hounsfield, the inventor of CT, is used. Water is assigned a value of 0 H, with the scale extending from –1,000 H for air to +3,000 H for very dense bone. H units are not absolute values but, rather, are relative values that may vary from one CT system to another. In general, cortical bone is +700 H, cancellous bone is +3,000 H, soft tissue is +40 to +80 H, fat is –90 to –120 H, lung is –500 H, and air is –1,000 H.

Voxel dimensions are determined by the computer algorithm chosen for reconstruction and the thickness of the scanned slice. Most CT units allow slice-thickness specifications between 0.5 and 10 mm. Data for an individual slice are routinely acquired in 1 second or less. Advantages of CT compared with MR include rapid scan acquisition, superior bone detail, and demonstration of calcifications. CT scanning is generally limited to the axial plane; however, images may be reformatted in sagittal, coronal, or oblique planes, or as three-dimensional images. Multidetector CT allows the acquisition of cube-shaped isotropic voxels of equal length on all three sides. Isotropic voxels allow direct image reconstruction in any plane without loss of resolution.

Conventional CT (single-slice CT) obtains image data one slice at a time. The patient holds his or her breath, a slice is taken, the patient breathes, the table moves, and the sequence is repeated. This technique requires at least two to three times the total scanning time of helical CT for any given patient scan volume, making optimization of scanning during maximum contrast more difficult. Minor changes in lung volume with each breath-hold may make substantial changes in the chest and abdomen anatomy scanned, resulting in "skip" areas. Conventional scanners have largely been replaced by multidetector helical CT scanners.

Helical CT, also called spiral CT, is performed by moving the patient table at a constant speed through the CT gantry while scanning continuously with an x-ray tube rotating around the patient. A continuous volume of image data is acquired during a single breath-hold. This technique dramatically improves the speed of image acquisition, enables scanning during optimal contrast opacification, and eliminates artifacts and errors caused by misregistration and variations in patient breathing. The entire liver may be scanned in a single breath-hold; the entire abdomen and pelvis, in one or two breath-holds, all with optimal timing for organ opacification following intravenous contrast administration. Volume acquisition enables retrospective reconstruction of multiple overlapping slices, improving visualization of small lesions and allowing high-detail three-dimensional CT angiography (Fig. 1.9). Scans can be obtained during multiple phases of organ enhancement; arterial, venous, parenchymal, delayed.

Multidetector helical CT (MDCT) was a major technical advance in CT imaging, utilizing the principles of the helical scanner but incorporating multiple rows of detector rings. This allows acquisition of multiple slices per tube rotation increasing the area of the patient that can be covered in a given time by the x-ray beam. Available systems have moved quickly from 2-slice to 256 to 320-slice, which can cover over 400 mm of patient length for each 1-second or less rotation of the tube. The key advantage of MDCT is speed. MDCT is many times faster than single-slice helical CT. For body scanning 1-mm slices can be obtained creating isotropic voxels (1 × 1 × 1 mm) allowing image reconstruction in any anatomic plane without loss of resolution. Broad area coverage allows for high detail CT angiography and "virtual" CT colonoscopy and bronchoscopy. Nothing is free, however, and a significant disadvantage of MDCT is radiation dose, which can be three to five times higher with MDCT than with single-slice CT. Thin slices and multiple acquisitions add great diagnostic capability but at the cost of increased radiation dose to the patient.

FIGURE 1.9. CT Angiogram. A three-dimensional, shaded surface display, angiogram image of the aorta and its branches was created from a series of axial plane MDCT images obtained during rapid bolus IV contrast agent administration. Intravenous contrast injection greatly increases the CT numbers of the arteries allowing removal of structures with lower CT density from the image by "thresholding." Only pixels with CT numbers higher than a specified threshold value are displayed. Computer algorithms create a "virtual" three-dimensional image from data provided by many overlapping axial slices. The three-dimensional image can be rotated and viewed from any desired angle on a computer monitor. "Shading," simulating light cast from a remote light source, enhances the three-dimensional visual effect. This patient has advanced atherosclerosis (atherosclerotic plaques are shown in white) and a small aneurysm (arrow) of the infrarenal abdominal aorta. The enhanced kidneys are partially shaded red.

CT fluoroscopy is another advancement in CT technology that allows for

real-time CT imaging. This technique dramatically improves the ability to perform percutaneous image-guided interventions quickly and at a generally moderate radiation dose. The operator can step on a floor pedal while moving the CT table or observing patient motion. Rapid image reconstruction provides real-time images of anatomy, lesions, and needle or catheter placement. CT fluoroscopy is now routinely used to guide biopsy, drainage, and interventional procedures anywhere in the body. It is particularly useful in guidance of needle placements where there is physiologic motion such as in the chest and abdomen.

Dual-energy CT (dual-source CT) utilizes two x-ray sources and two x-ray detectors to simultaneously interrogate tissues to determine how tissue behaves at different radiation energies. This technique adds information about tissue composition. Differences in fat, soft tissue, and contrast agents at different energy levels expand lesion conspicuity and characterization. Image data can be captured in half the time required for conventional MDCT. This vastly improves the ability to image the heart without the use of potentially dangerous beta-blockers to slow the heart rate. The chemical composition of urinary calculi can be determined allowing selection of medical versus surgical treatment.

Contrast Administration in CT. Intravenous iodine-based contrast agents are administered intravenously during CT to enhance density differences between lesions and surrounding parenchyma, to demonstrate vascular anatomy and vessel patency, and to characterize lesions by their patterns of contrast enhancement. Optimal use of intravenous contrast depends upon the anatomy, physiology, and pathology of the organ of interest. In the brain the normal blood–brain barrier of tight neural capillary endothelial junctions prevents access of contrast into the neural extravascular space. Defects in the blood–brain barrier associated with tumors, stroke, infection, and other lesions enable contrast accumulation within abnormal tissue, improving its visibility. In nonneural tissues, the capillary endothelium has loose junctions, enabling free access of contrast into the extravascular space. Contrast administration and timing of CT scanning must be carefully planned to optimize differences in enhancement patterns between lesions and normal tissues. For example, most liver tumors are predominantly supplied by the hepatic artery, whereas the liver parenchyma is predominantly supplied by the portal vein (~70%), with a lesser contribution from the hepatic artery (~30%). Contrast given by bolus injection in a peripheral arm vein will arrive

earliest in the hepatic artery and enhance (i.e., increase the CT density of) many tumors to a greater extent than the liver parenchyma. Maximal enhancement of the liver parenchyma is delayed 1 to 2 minutes until the contrast has circulated through the intestinal tract and spleen and is returned to the liver via the portal vein. Differentiation of tumor and parenchyma by contrast enhancement can thus be maximized by giving an IV bolus of contrast and by performing rapid CT scanning of the liver early during maximum arterial enhancement and delayed scanning during maximum portal venous enhancement. MDCT is ideal for this early and rapid scanning of the liver. Oral or rectal contrast is generally required to opacify the bowel for CT scans of the abdomen and pelvis. Bowel without intraluminal contrast may be difficult to differentiate from tumors, lymph nodes, and hematoma.

CT Artifacts. Artifacts refer to components of the image that do not faithfully reproduce actual anatomic structures because of distortion, addition, or deletion of information. Artifacts degrade the image and may cause errors in diagnosis.

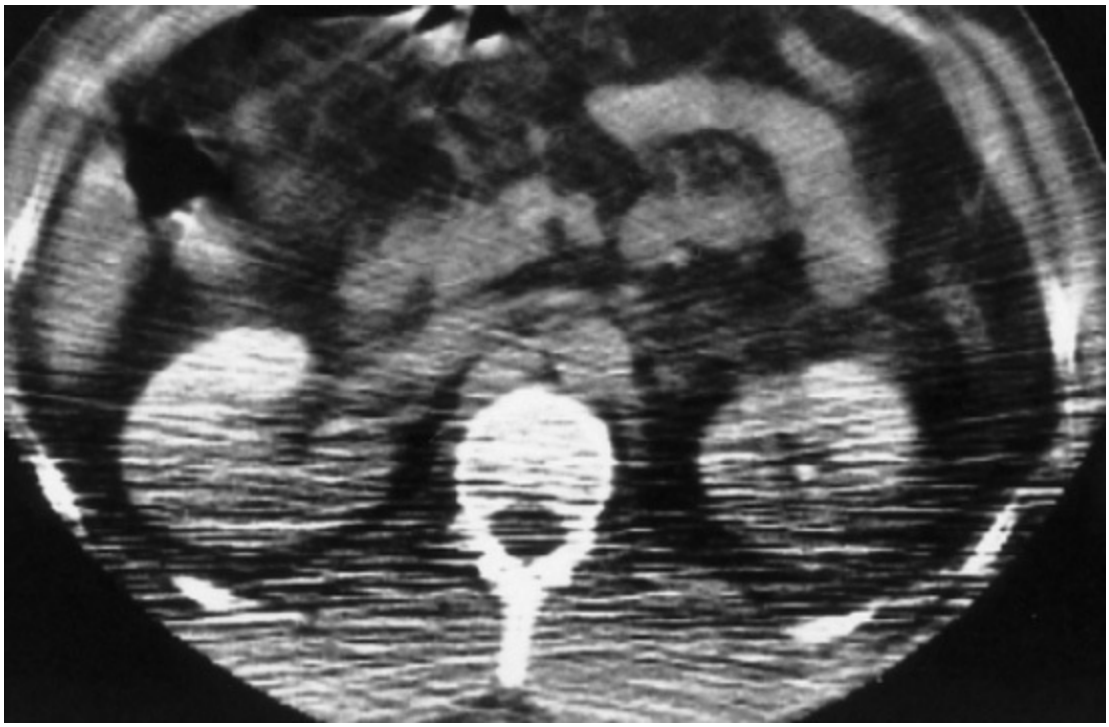

FIGURE 1.10. Beam Hardening Artifact. A CT image of the abdomen is severely degraded by beam hardening artifact that produces dark streaks across the lower half of the image. The artifact was caused by marked attenuation of the x-ray beam by the patient's arms, which were kept at his sides owing to injury.

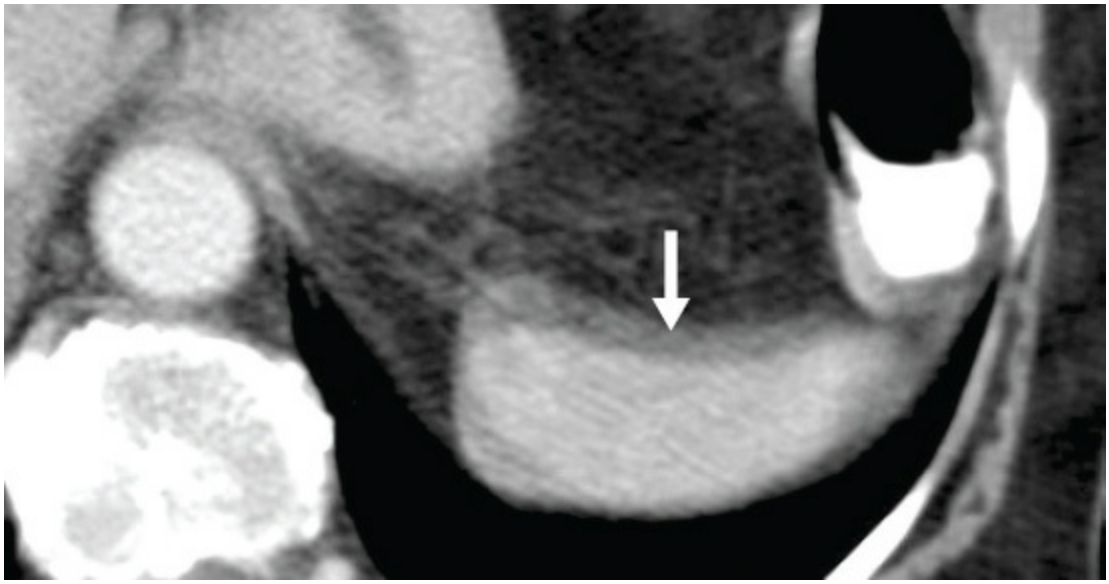

FIGURE 1.11. Motion Artifact. Breathing motion during image acquisition duplicates the margin (arrow) of the spleen simulating a subcapsular hematoma in this patient imaged because of abdominal trauma.

Volume averaging is present in every CT image and must always be considered in image interpretation. The displayed two-dimensional image is created from data obtained and averaged from a three-dimensional volume of patient tissue. Slices above and below the image being interpreted must be examined for sources of volume averaging that may be misinterpreted as pathology.

Beam hardening artifact results from greater attenuation of low-energy x-ray photons than high-energy x-ray photons as they pass through tissue. The mean energy of the x-ray beam is increased (the beam is "hardened"), resulting in less attenuation at the end of the beam than at its beginning. Beam-hardening errors are seen as areas or streaks of low density (Fig. 1.10) extending from structures of high x-ray attenuation such as the petrous bones, shoulders, and hips, or concentrations of contrast agents.

Motion artifact results when structures move to different positions during image acquisition. Motion occurs as a result of voluntary or involuntary patient movement, breathing, heartbeat, vessel pulsation, or peristalsis. Motion is demonstrated in the image as prominent streaks from high- to low-density interfaces or as blurred or duplicated images (Fig. 1.11).

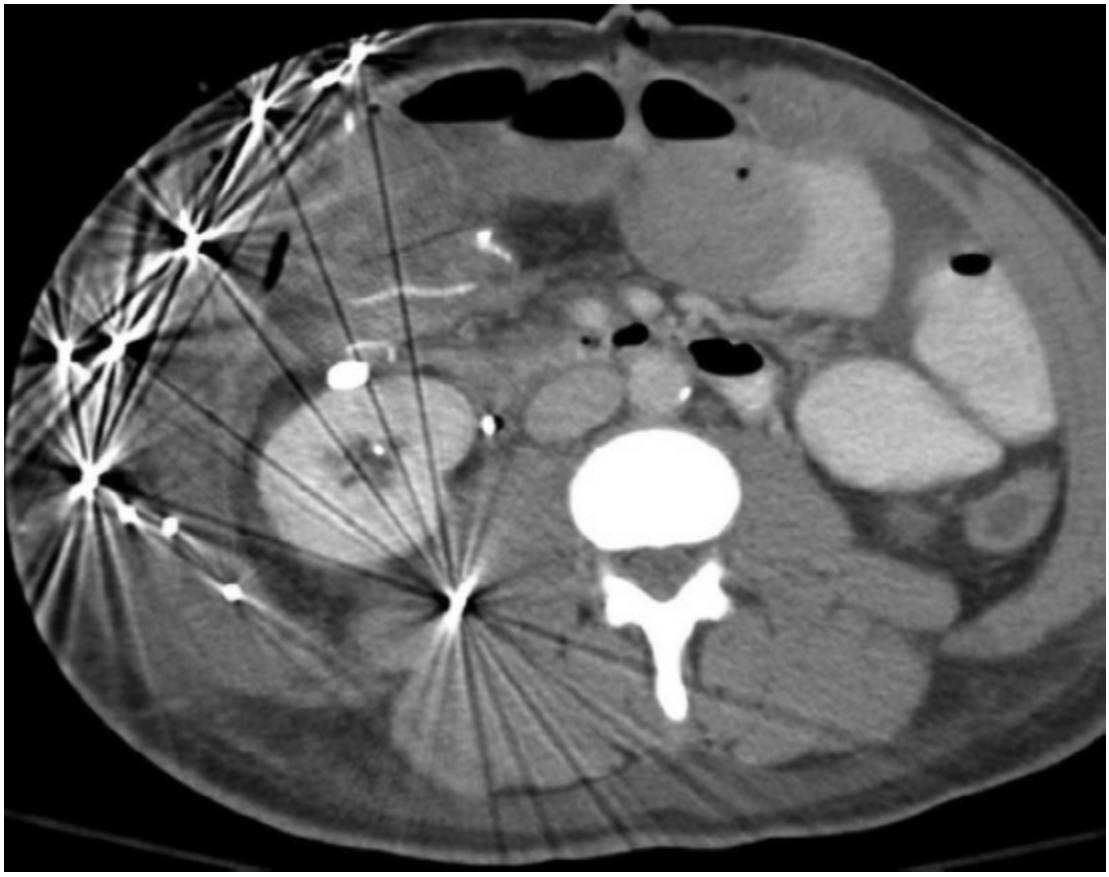

FIGURE 1.12. Streak Artifact. Shotgun pellets produce severe streak artifact on this CT image.

Streak artifacts emanate from high-density sharp-edged objects such as vascular clips and dental fillings (Fig. 1.12). Reconstruction algorithms cannot handle the extreme differences in x-ray attenuation between very dense objects and adjacent tissue.

Ring artifacts occur when the CT scanner is out of calibration and detectors give erroneous readings at each angle of rotation. Ring artifacts are seen as high- or low-density circular rings in the image.

Quantum mottle artifacts produce noise in the image seen as salt and pepper pattern of random dark and light specks throughout the image. The image noise results from insufficient x-ray transmission data caused by inappropriate radiation settings for the location of scanning and the size of the patient.

Principles of CT Interpretation. Like all imaging analysis, CT interpretation is based on an organized and comprehensive approach. CT images are viewed in sequential anatomic order, examining each slice with reference to slices above and below. This image analysis is made dramatically easier by viewing CT images on a PACS workstation. The

interpreting physician can scroll up and down the stacked image display. The radiologist must seek to develop a three-dimensional concept of the anatomy and pathology displayed. This analysis is fostered by the availability of images obtained or reconstructed in coronal and sagittal, as well as axial planes. The study must be interpreted with reference to the scan parameters, slice thickness and spacing, administration of contrast, timing of scanning relative to contrast enhancement, and presence of artifacts. Axial images are oriented so that the observer is looking at the patient from below. The patient's right side is oriented on the left side of the image. Optimal bone detail is viewed at "bone windows," generally a window width of 2,000 H and a window level of 400 to 600 H. Lungs are viewed at "lung windows" with a window width of 1,000 to 2,000 H and window levels of –500 to –600 H. Soft tissues are examined at window width 400 to 500 H and window level 20 to 40 H. Narrow windows (width = 100 to 150 H, level = 70 to 80 H) increase image contrast and aid in the detection of subtle liver and spleen lesions. PACS workstation viewing of digital images allows the interpreter to actively manipulate the image, magnify, change image brightness and contrast, measure attenuation, and to create oblique and three-dimensional image reconstructions to optimize interpretation.

Magnetic Resonance Imaging

MR is a technique that produces tomographic images by means of magnetic fields and radiowaves. Although CT evaluates only a single tissue parameter, x-ray attenuation, MR analyzes multiple tissue characteristics including hydrogen (proton) density, T1 and T2 relaxation times of tissue, and blood flow within tissue. The soft tissue contrast provided by MR is substantially better than for any other imaging modality. Differences in the density of protons available to contribute to the MR signal discriminate one tissue from another. Most tissues can be differentiated by significant differences in their characteristic T1 and T2 relaxation times. T1 and T2 are features of the three-dimensional molecular environment that surrounds each proton in the tissue imaged. T1 is a measure of a proton's ability to exchange energy with its surrounding chemical matrix. It is a measure of how quickly a tissue can become magnetized. T2 conveys how quickly a given tissue loses its magnetization. Blood flow has a complex effect on the MR signal that may decrease or increase signal intensity within blood vessels.

The complex physics of MR is beyond the scope of this book but is reviewed

in detail in the text Essentials of Body MRI. In simplest terms, MR is based on the ability of a small number of protons within the body to absorb and emit radiowave energy when the body is placed within a strong magnetic field. Different tissues absorb and release radiowave energy at different, detectable, and characteristic rates. MR scans are obtained by placing the patient in a static magnetic field 0.02 to 3 Tesla (T) in strength, depending on the particular MR unit used. Scanners using a magnetic field of 1.5 T are most common. MR scanners at 4 T, 7 T, 8 T, and 9.4 T are being developed. Low-field strength systems (<0.1 T), midfield systems (0.1 to 1.0 T), and high-field systems (1.5 T and 3.0 T) each have their own advantages and disadvantages. The choice of unit for imaging is based on preference and local availability. A small number of tissue protons in the patient align with the main magnetic field and are subsequently displaced from their alignment by application of radiofrequency (RF) gradients. When the RF gradient is terminated, the displaced protons realign with the main magnetic field, releasing a small pulse of energy that is detected, localized, and then processed by a computer algorithms similar to those used in CT to produce cross-sectional tomographic anatomic images. Slice location is determined by application of a slice selection gradient of gradually increasing intensity along the z-axis, defined as being parallel to the direction of the scanner's static magnetic field. The small energy pulses released by tissue protons are further localized by "frequency-encoding" in one direction (x-axis) and "phase-encoding" in the other direction (y-axis). Images can be obtained in any anatomic plane by adjusting the orientation of the x-axis, y-axis, and z-axis magnetic field gradients. Because the MR signal is very weak, prolonged imaging time is often required for optimal images. Standard spin-echo sequences produce a batch of images in 10 to 20 minutes. Rather than obtaining data for each image one slice at a time, many spin-echo MR sequences obtain data for all slices in the imaged tissue volume throughout the entire imaging time. Thus, motion caused by breathing and cardiac and vascular pulsation may degrade the image substantially. MR has advanced to rapid imaging breath-hold techniques using gradient recalled echo (GRE), echo train, and echo-planar sequences. Continued rapid-paced technologic improvements are making MR acquisition times comparable with those for CT.

Present MR technology relies on a variety of MR sequence techniques, with many variations used by different MR manufacturers (Fig. 1.13) . Acronyms rule.

Spin-echo (SE) pulse sequences produce standard T1-weighted images (WI), T2WI, and proton density–weighted images. T1WI emphasize differences in the T1 relaxation times between tissues, while minimizing differences in T2 times. On the resultant image tissues with short T1 values are relatively bright (high signal intensity), while those with long T1 times are relatively dark (low signal intensity). T1WI usually provide the best anatomic detail and are good for identifying fat, subacute hemorrhage, and proteinaceous fluids. T2WI emphasize differences in the T2 relaxation times of tissues while minimizing differences in T1 times. Tissues with long T2 times are relatively bright, while those with short T2 times are relatively dark. T2WI usually provide the most sensitive detection of edema and pathologic lesions. Proton density–weighted images accentuate proton density differences in tissues and are most useful in brain imaging.

Two major components of MR instrument settings selected by the operator for SE sequences are TR and TE. The time between administered RF pulses, or the time provided for protons to align with the main magnetic field, is TR (time of repetition). The time provided for absorbed radiowave energy to be released and detected is TE (time of echo). Spin-echo T1WI are obtained by selecting short TR (~500 ms) and short TE (~20 ms) settings. Spin-echo T2WI use a long TR (≥2,000 ms) and long TE (≥70 ms). Proton density–weighted images use a long TR (2,000 to 3,000 ms) and a short TE (25 to 30 ms) to minimize T1 and T2 effect and accentuate hydrogen-density differences in tissues.

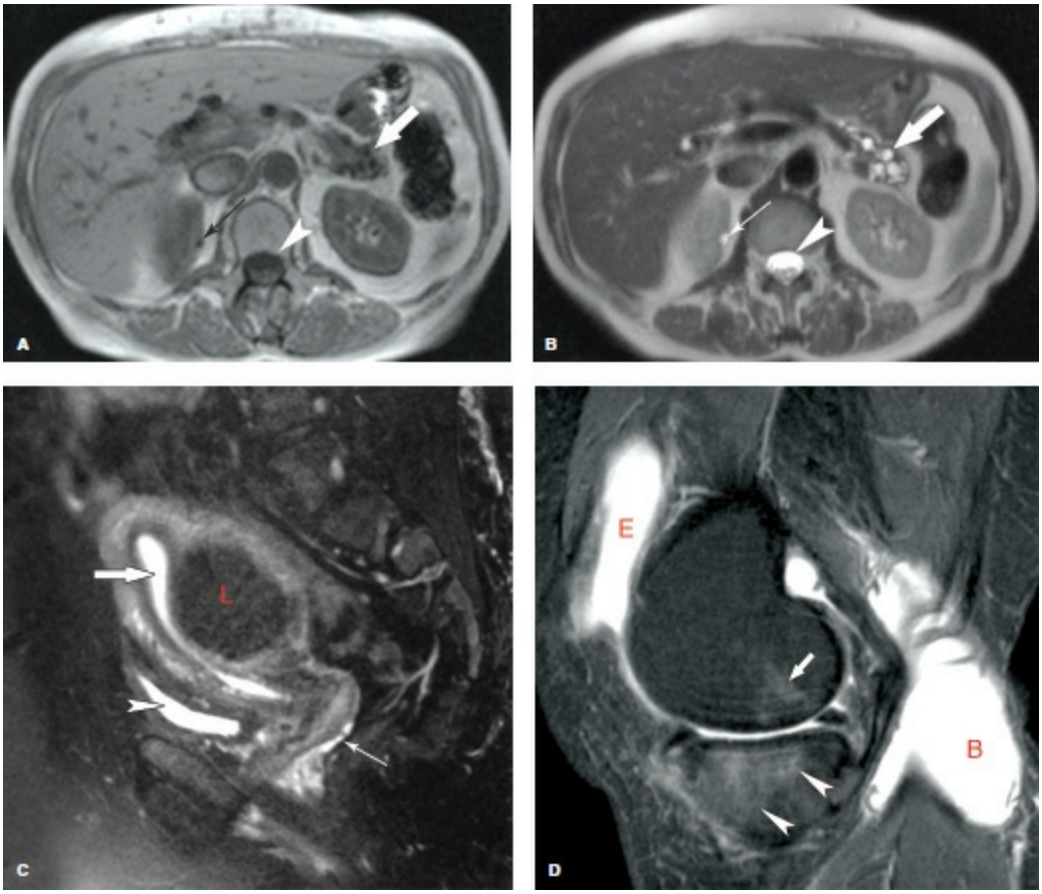

FIGURE 1.13. MR Sequences. Gradient recall in-phase T1WI, **A**, and HASTE T2WI, **B**, taken at the same slice location demonstrates dark signal in free water on T1WI and bright signal of free water on T2WI. Note the improved conspicuity of the cystic lesion (thick arrows) of the pancreas on the T2WI compared to the T1WI. The cerebrospinal fluid (arrowheads) in the spinal canal also shows marked increase in signal on T2WI. A tiny cyst (skinny arrows) in the right kidney is confirmed as benign by showing the signal intensities of simple free water (dark on T1WI, bright on T2WI). **C:** Sagittal turbo spin-echo (TSE) T2WI with fat saturation shows a low signal leiomyoma (L) and bright signal from fluid in the endometrial canal (thick arrow) and from urine in the bladder (arrowhead). A small amount of fluid is evident in the cul-de-sac (skinny arrow), a normal finding in a woman of child-bearing age. Note the lack of signal from fat as compared to **B**, the T2WI without fat saturation. **D:** Sagittal plane STIR image of the knee accentuates bright signal from free water in the knee effusion (E), Baker cyst (B), and bone bruise edema in the femoral condyle (arrow) and tibial plateau (arrowheads).

Multiple spin-echo sequences, also known as echo-train, rapid-acquisition relaxation-enhanced (RARE), fast spin-echo (FSE), or turbo spin-echo (TSE) sequences, significantly reduce image acquisition time. Signal intensity is less than with SE sequences and image blurring occurs. Fat is bright on T2WI impairing detection of pathology, such as edema in fat adjacent to an inflammatory process. Addition of fat-suppression techniques counters this effect. Fast low-angle acquisition with relaxation enhancement (FLARE) and half-Fourier acquisition single-shot turbo spin echo (HASTE) are variations of

this technique.

Inversion recovery (IR) pulse sequences are used mainly to emphasize differences in T1 relaxation times of tissues. A delay time, TI (time of inversion) is added to the TE and TR instrument settings selected by the operator. Standard IR sequences, using a long TI, produce T1WI. Tissues with short T1 times yield a brighter signal. Short TI inversion recovery (STIR) sequences are the most commonly used. This sequence achieves additive T1-weighted, T2-weighted, and proton density weighted contrast to increase lesion conspicuity. With STIR sequences, all tissues with short T1 relaxation times, including fat, are suppressed, whereas tissue with high water content, including many pathologic lesions, are accentuated, yielding a bright signal on a dark background of nulled short-T1 tissue. STIR images more closely resemble strongly T2WI.

Gradient recalled echo (GRE) pulse sequences are used to perform fast MR and MR angiography. Rapid image sequences are particularly useful in body MR to minimize motion artifact of breathing, heartbeat, vessel pulsation, and bowel peristalsis. T1-weighted GRE sequences have completely replaced SE T1-weighted sequences in body MR imaging. Partial "flip angles" of less than 90 degrees are used to decrease the time to signal recovery. Signal intensity arising from T2 relaxation characteristics of tissue is strongly affected by imperfections in the magnetic field on GRE images. Magnetization decay time with GRE imaging is termed T2* ("T2 star") and is much shorter than the "true" T2 decay times seen with SE imaging. T2*-weighted imaging are used to depict hemorrhage, calcification, and iron deposition in tissues. GRE images are characteristically low in image contrast, have more prominent artifacts, and demonstrate flowing blood with bright signal. T1-, T2-, T2*-, and proton density–image weighting is determined by the combination of flip angle, TR, and TE settings. Fast GRE techniques include fast low-angle shot (FLASH), gradient-recalled acquisition in steady state (GRASS), and true fast imaging with steady-state precession (FISP), snapshot FLASH, rapid acquisition with gradient echo (RAGE) and magnetization prepared RAGE (MPRAGE).

Echo-planar imaging is a very fast MR technique that can produce single-slice images in 20 to 100 ms. All spatial encoding information is obtained after a single RF excitation, compared with the multiple RF excitations separated by TR intervals required for conventional MR. Motion artifact is virtually eliminated, and moving structures can be "freeze-frame" imaged.

Special hardware is required for echo-planar imaging, but standard SE, GRE, and IR pulse sequences can be obtained. Echo-planar imaging overcomes many of the time and motion limitations of conventional MR and enables expansion of MR to new areas such as blood perfusion and cortical activation of the brain.

Diffusion-weighted imaging (DWI) sequences are designed to detect alteration in the random (brownian) motion of water molecules within tissues. DWI measures diffusion, the mean path length traveled by water molecules within a specific time interval. DWI techniques were initially applied to neuroradiology particularly in detection of acute cerebral ischemia but have become increasing useful in body imaging for tumor detection, tumor characterization, and evaluation of tumor response to treatment.

Diffusion-tensor imaging (DTI) and fiber tractography demonstrate the orientation and integrity of white matter fibers particularly useful in diagnosis of diseases of the corpus callosum and in cortical dysplasia. DTI also has application in imaging muscle fibers in the heart and musculoskeletal system.

MR spectroscopy provides demonstration of relative tissue metabolite concentrations based on chemical shift phenomena. Choline, creatine, citrate, lactate, and other metabolites change in different pathologic conditions. For example, in the breast peaks of choline suggest malignancy. MR spectroscopy has expanding utility in diagnosis of conditions in the brain, breast, abdominal organs, and musculoskeletal system.

Fat-suppression techniques are used in MR to detect the presence of fat or to suppress signal from fat to enhance detection of pathology (tumor invasion into fat or edema in fat).

Fat-saturation technique takes advantage of the difference in resonance frequencies of water and fat. Signal from fat is suppressed while the image is produced from the remaining signal of water. Fat-saturation technique modifies only the signal of fat without modifying signal characteristics of other tissues. It can be used effectively with contrast-enhanced images. This technique is highly sensitive to magnetic field inhomogeneity and misregistration artifacts, and does not work well with low-field magnets. The technique is optimal for suppressing signal from macroscopic fat within adipose tissue (Fig. 1.13C).

Short TI Inversion Recovery (STIR) provides global homogeneous fat suppression but suppresses all tissues with very short T1, including tissue enhanced by administration of intravenous gadolinium, mucoid tissue,

hemorrhage, and proteinaceous fluid (Fig. 1.13D). It can be used with low-field magnets and is insensitive to inhomogeneities in the magnetic field.

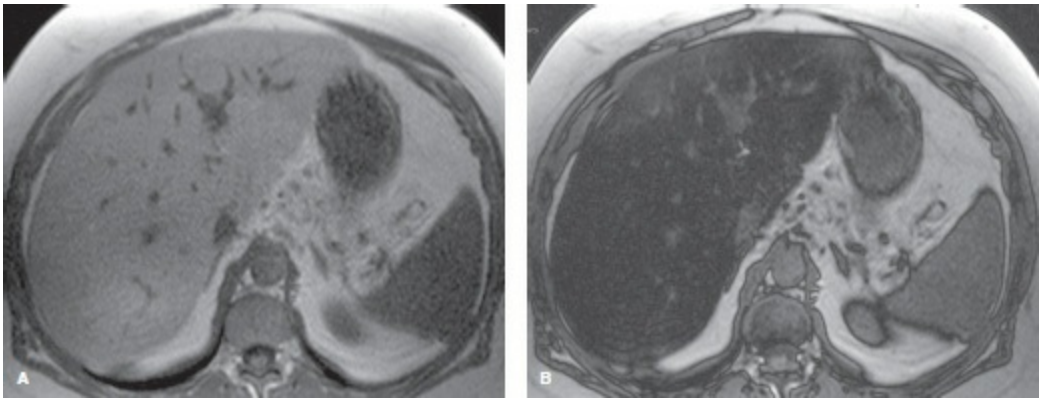

FIGURE 1.14. Opposed Phase Fat-Suppression Technique. Compare the in-phase image of the liver, **A**, with the opposed phase image of the liver, **B**. The dramatic darkening of the liver on the opposed phase image is indicative of diffuse fatty infiltration. The signal from fat within hepatocytes is subtracted from the total signal including fat and water on the in-phase image.

Chemical shift imaging (opposed phase MR) is fast, reliable, and optimal for detection of small amounts of fat such as intracellular fat in adrenal adenomas and fatty-infiltrated hepatocytes in the liver (Fig. 1.14). Resonance frequency of water is different (faster than) that of fat. In-phase (IP) images add signal from fat and water. Opposed phase (out-of-phase [OP]) images subtract water signal from fat signal. The presence of fat within cells is demonstrated by a distinct drop in signal intensity on the OP image compared to the IP image. Chemical shift imaging is characterized by two distinctive edge artifacts. The technique results in spatial misregistration of fat signal resulting in alternating bands of bright and dark signal at water/fat interfaces in the frequency-encoded direction. The second artifact is a thin black line at interface between fat and water laden tissue (e.g., the interface between the kidney and perinephric fat) has been termed the "india ink artifact." This artifact is useful in identification of the OP image and may additionally be used to identify fatty tumors such as angiomyolipomas. The india ink artifact occurs along the entire border between fat and water (fat/organ, fat/muscle), not only in the frequency-encoded direction. The artifact results from the presence of fat and water molecules in the same voxel resulting in loss of signal by phase cancellation in all directions. Adipose tissue contains abundant fat and little water so the signal is minimally reduced on OP images. However, tissue with low fat content but high water content (adrenal adenomas, fat-infiltrated hepatocytes) shows a prominent loss of signal on

OP images compared to IP images. The obvious limitation is that opposed phase MR does not suppress signal from adipose tissue (Fig. 1.14B).

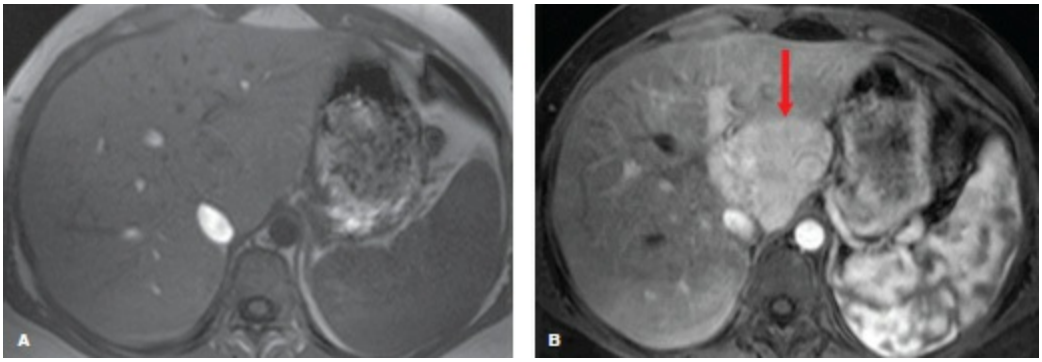

FIGURE 1.15. Contrast Administration in MR. Intravenous administration of gadolinium chelate dramatically increases the conspicuity of the liver mass (arrow) on an early postcontrast image, **B**, compared to a noncontrast image, **A**. The mottled enhancement of the spleen is caused by the relatively slow diffusion of contrast through the splenic sinusoids.

Advantages of MR include its outstanding soft tissue contrast resolution, ability to provide images in any anatomic plane, and absence of ionizing radiation. MR is limited in its ability to demonstrate dense bone detail or calcifications, has long imaging times for many pulse sequences, limited spatial resolution compared with CT, limited availability in some geographic areas, and is expensive. Because of the physically confining space for the patient within the magnet, a number of patients experience symptoms of claustrophobia and require sedation or are simply unable to tolerate MR scanning. "Open" magnet design aids in the MR imaging of very large and claustrophobic patients but these units are generally of lower-field strength and lack the resolution of the high-field strength "tube" magnets.

Contrast Administration in MR. Gadolinium chelates are used, similar to the use of iodinated contrast agents in CT, to identify blood vessels and confirm their patency, to identify regions of disruption of the blood–brain barrier, to enhance organs to accentuate pathology (Fig. 1.15), and to document patterns of lesion enhancement. Gadolinium is a rare-earth heavy metal ion with paramagnetic effect that shortens the T1 and T2 relaxation times of hydrogen nuclei within its local magnetic field. Gadolinium is important in providing high-quality MR angiographic studies by enhancing the signal differences between blood vessels and surrounding tissues. At recommended doses, gadolinium shortens T1 to a much greater extent than it shortens T2. Increases in signal intensity resulting from T1 shortening

resulting from concentrations of gadolinium are best seen on T1WI. However, when very high tissue concentration is reached, such as in the renal collecting system, T2 shortening causes a significant loss of signal intensity that is best seen on T2WI. Like iodinated contrast agents used in CT and radiography, gadolinium-based agents have potential adverse effects that must be considered before administration to patients.

Safety Considerations. The MR environment creates potential risks not only to the patient being imaged but also accompanying family members and healthcare personnel. MR is contraindicated in patients who have electrically, magnetically, or mechanically activated implants including cardiac pacemakers, insulin pumps, cochlear implants, neurostimulators, bone-growth stimulators, and implantable drug infusion pumps. Patients with intracardiac pacing wires or Swan–Ganz catheters are at risk for RF current-induced cardiac fibrillation and burns. Ferromagnetic implants such as cerebral aneurysm clips, vascular clips, and skin staples are at risk for rotation and dislodgment, burns, and induced electrical currents. Bullets, shrapnel, and metallic fragments may move and cause additional injury or become projectiles in the magnetic field. Metal workers and patients with a history of penetrating eye injuries should be screened with radiographs of the orbits to detect intraocular metallic foreign bodies that may dislodge, tear the retina, and cause blindness. Certain transdermal-medicated patches contain traces of aluminum and other metals in the adhesive backing. If worn during MR imaging skin burns may occur at the patch site. A variety of implantable devices have been confirmed to be safe for MR, including nonferromagnetic vascular clips and staples, orthopedic devices composed of nonferromagnetic materials, and a variety of noncardiac implantable pacemakers and stimulators. Each device must be checked for its MR compatibility. Prosthetic heart valves with metal components and stainless steel Greenfield filters are considered safe because the in vivo forces affecting them are stronger than the deflecting forces of the electromagnetic field. No convincing body of evidence indicates that short-term exposure to the electromagnetic fields of MR harms the developing fetus, although it is not possible to prove that MR is absolutely safe in pregnancy. Pregnant patients can be scanned, provided the study is medically indicated. In the event of a cardiac arrest the patient must be removed from the MR magnet room to run cardiopulmonary resuscitation.

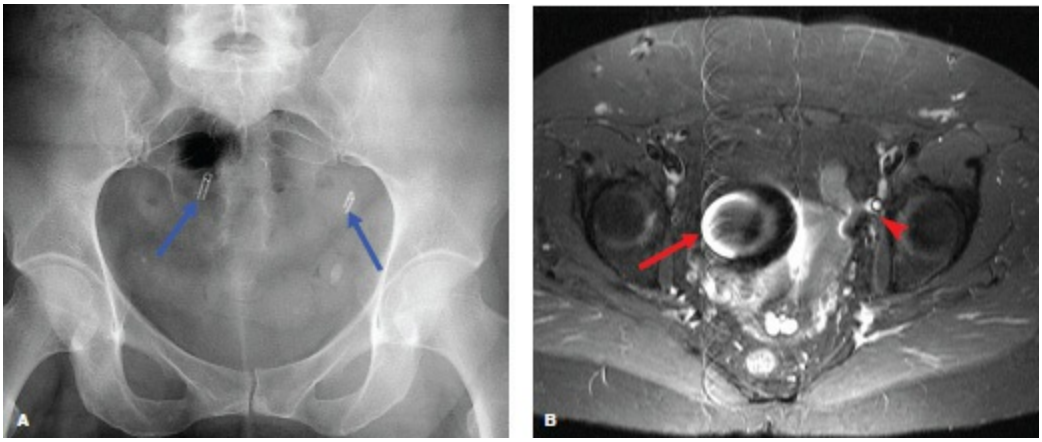

FIGURE 1.16. Magnetic Susceptibility Artifact. Radiograph of the pelvis, **A**, and axial plane T2-weighted MR image, **B**, in the same patient show the artifact (red arrow, red arrowhead) produced by metallic clips (blue arrows) used for tubal ligation. The dramatic increase in artifact on the right side (red arrow) as compared to the left side (red arrowhead) is caused by proximity of the right-sided clip to a blood vessel creating pulsatile motion of the clip.

MR Artifacts. Artifacts are intrinsic to MR technique and must be recognized to avoid mistaking them for disease.

Magnetic susceptibility artifact is caused by focal distortions in the main magnetic field resulting from the presence of ferromagnetic objects such as orthopedic devices, surgical clips and wires, dentures, metallic foreign bodies in the patient, and ingested material, such as various forms of iron tablets. The artifact is seen as areas of signal void at the location of the metal implant (Fig. 1.16), often with a rim of increased intensity and a distortion of the image in the vicinity.

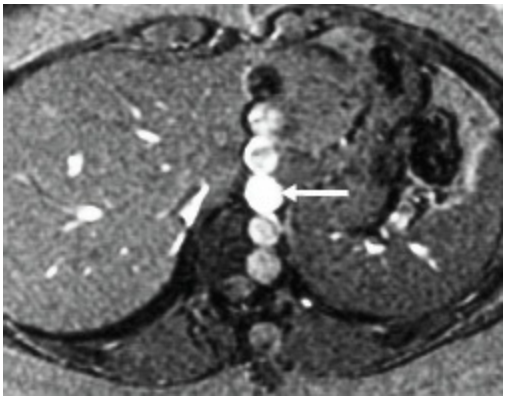

FIGURE 1.17. Motion Artifact. Pulsations of the aorta (arrow) produce numerous ghosts of the aorta in the phase-encoded direction. Swapping the phase-encoded direction with the frequency-encoded direction will enable evaluation of the left lobe of the liver.

Motion artifact is common in MR when image acquisition time is long. Random motion produces blurring of the image. Periodic motion, such as that caused by pulsating blood vessels, causes ghosts of the moving structures (Fig. 1.17) . Motion artifacts are most visible along the phase-encoded direction. Swapping phase- and frequency-encoded directions may make the artifacts less bothersome.

Chemical shift misregistration occurs at interfaces between fat and water. Protons bound in lipid molecules experience a slightly lower magnetic influence than protons in water when exposed to an externally applied gradient magnetic field, resulting in misregistration of signal location. The artifact is seen as a line of high-signal intensity on one side of the fat–water interface and a line of signal void at the opposite side of the fat–water interface (Fig. 1.18) . Evaluation of the bladder wall and renal margins is difficult in the presence of this artifact.

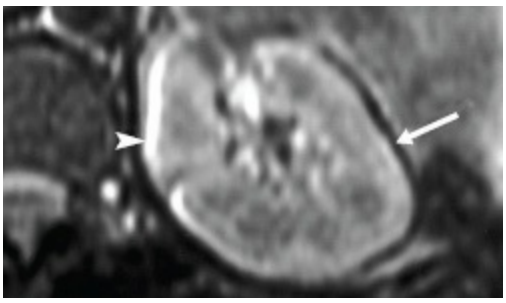

FIGURE 1.18. Chemical Shift Artifact. Chemical shift misregistration between fat and kidney tissue produces a high-density band (arrowhead) on the medial aspect of the left kidney and a low-density band (arrow) on its lateral aspect.

Truncation error occurs adjacent to sharp boundaries between tissues of markedly different contrast. The artifact is attributable to inherent errors in the Fourier transform technique of image reconstruction. The artifact appears as regularly spaced alternating parallel bands of bright and dark signal. It may simulate a syrinx of the spinal cord or a meniscal tear in the knee.

TABLE 1.1

RULES OF MR SOFT TISSUE CONTRAST

T1-Weighted Images		
Short T1 tissue	⇒	High signal
Long T1 tissue	⇒	Low signal
T2-Weighted Images		
Short T2 tissue	⇒	Low signal
Long T2 tissue	⇒	High signal

Aliasing, or image wraparound, artifact occurs when anatomy outside the designated field of view but within the image plane is mismapped onto the opposite side of the image, for instance, on a midline sagittal brain MR, the patient's nose may be artifactually displayed over the area of the posterior fossa. Aliasing may be eliminated by increasing the field of view (at the expense of loss of image resolution) or by increasing the number of phase-encoding steps outside the field of view (oversampling).

Principles of MR Interpretation. Outstanding soft tissue contrast is obtained in MR by designing imaging sequences that accentuate differences in T1 and T2 tissue relaxation times. Sequences that accentuate differences in proton density are fruitful in brain imaging but are generally less useful for extracranial soft tissue imaging, in which proton density differences are small. Interpreting MR depends on a clear understanding of the biophysical basis of MR tissue contrast. Water is the major source of the MR signal in tissues other than fat. Mineral-rich structures such as bone and calculi, and collagenous tissues such as ligaments, tendons, fibrocartilage, and tissue fibrosis, are low in water content and lack mobile protons to produce an MR signal. These tissues are low in signal intensity on all MR sequences. Water in tissue exists in at least two physical states: free water with unrestricted motion and bound water with restricted motion owing to hydrogen bonding with proteins. Free water is found mainly in extracellular fluid, whereas bound water is found mainly in intracellular fluid. Intracellular water is both bound and free and is in a condition of rapid exchange between the two states.

Free water has long T1 and T2 relaxation times, resulting in low signal intensity on T1WI and high signal intensity on T2WI (Table 1.1). Organs with abundant extracellular fluid, and therefore large amounts of free water, include kidney (urine); ovaries and thyroid (fluid-filled follicles); spleen and penis (stagnant blood); and prostate, testes, and seminal vesicles (fluid in tubules) (Table 1.2). Edema is an increase in extracellular fluid and tends to have the effect of prolonging T1 and T2 relaxation times in affected tissues.

Most neoplastic tissues have an increase in extracellular fluid as well as an increase in the proportion of intracellular free water, resulting in their visualization with bright signal intensity on T2WI. In organs, such as the kidney, that are also rich in extracellular or free water, neoplasms may appear isointense or hypointense compared with the bright normal parenchyma on T2WI. Neoplasms that are hypocellular or fibrotic have low signal intensity on T2WI because fibrous tissue dominates their signal characteristics. Simple cysts, cerebrospinal fluid, urine in the bladder, and bile in the gallbladder all reflect the signal characteristics of free water.

TABLE 1.2

MR SIGNAL STRENGTH OF TISSUES AND BODY FLUIDS

TISSUE/BODY FLUID	EXAMPLES	T1WI SIGNAL	T2WI SIGNAL
Gas	Air in the lung Gas in the bowel	Absent	Absent
Mineral rich tissue	Cortical bone Calculi	Absent	Absent
Collagenous tissue	Ligaments, tendons Fibrocartilage, scar tissue	Low	Low
Fat	Adipose tissue Fatty bone marrow	High	Intermediate to high
High bound water tissue	Liver, pancreas, adrenal Muscle, hyaline cartilage	Low	Low to intermediate
High free water tissue	Kidney, testes, prostate Seminal vesicles, ovary Thyroid, spleen, penis Bladder, gallbladder, edema	Low	High
Fluid	Urine, bile Simple cysts	Black	White
Proteinaceous fluid	Complicated cyst, abscess Synovial fluid, nucleus pulposus	Intermediate	High
Brain tissue/fluid	Gray matter White matter Ventricles/cerebrospinal fluid	Low High Black	High Low White

Modified from Mitchell DG, Burk DL Jr, Vinitski S, Rifkin MD. The biophysical basis of tissue contrast in extracranial MR imaging. *AJR Am J Roentgenol* 1987;149:831–837 and Atlas SW, ed. *Magnetic Resonance Imaging of the Brain and Spine*. 4th ed. Philadelphia, PA: Lippincott Williams & Wilkins; 2009.

Proteinaceous Fluids. The addition of protein to free water has the effect of shortening the T1 relaxation time, thus brightening the signal on T1WI. T2 relaxation is also shortened, but the T1 shortening effect is dominant even on T2WI. Therefore, proteinaceous fluid collections remain high in signal intensity on T2WI. Proteinaceous fluids include synovial fluid, complicated cysts, abscesses, many pathologic fluid collections, and necrotic areas within tumors.